Optimization of state-of-the-art fuzzy-metaheuristic ANFIS based machine learning models for flood susceptibility prediction mapping in the Middle Ganga Plain, India

Aman Arora[1], Alireza Arabameri[2], Manish Pandey[3*], Masood A. Siddiqui[1], U.K. Shukla[5], Dieu Tien Bui[6], Varun Narayan Mishra[7], Anshuman Bhardwaj[8]*

[1]Department of Geography, Faculty of Natural Sciences, Jamia Millia Islamia, New Delhi-110025

[2]Department of Geomorphology, Tarbiat Modares University, Jalal Ale Ahmad Highway, Tehran 9821, Iran

[3]University Center for Research & Development (UCRD), Chandigarh University, Mohali-140413, Punjab, India

[4]Department of Civil Engineering, Chandigarh University, Mohali-140413, Punjab, India

[5]Center for Advanced Study in Geology, Institute of Science, Banaras Hindu University, Varanasi-221005, India

[6]Institute of Research and Development, Duy Tan University, Da Nang 550000, Vietnam

[7]Centre for Climate Change and Water Research, Suresh Gyan Vihar University, Jaipur-302017, Rajasthan, India

[8]School of Geosciences, University of Aberdeen, Meston Building, King's College, Aberdeen, AB24 3UE, UK

[*]Corresponding author: manish07sep@gmail.com; aman.jmi01@gmail.com

Abstract

This study is an attempt to quantitatively test and compare novel advanced-machine learning algorithms in terms of their performance in achieving the goal of zonation of predicting flood susceptible areas in a low altitudinal range, sub-tropical floodplain environmental setting like that prevailing in the Middle Ganga Plain (MGP), India. This part of the Ganga floodplain region, which under the influence of undergoing active tectonic regime related subsidence, is the hotbed of annual flood disaster, and is one of the best natural laboratories to test the flood susceptibility models for establishing a universalization of such models in low relief highly flood prone areas. Based on highly sophisticated flood inventory archived for this region, and 12 flood conditioning factors viz. annual rainfall, soil type, stream density, distance from stream, distance from road, Topographic Wetness Index (TWI), altitude, slope aspect, slope, curvature, land use/land cover, and geomorphology, an advanced novel hybrid model Adaptive Neuro Fuzzy Inference System (ANFIS), and three metaheuristic models-based ensembles with ANFIS namely ANFIS-GA (Genetic Algorithm), ANFIS-DE (Differential Evolution), and ANFIS-PSO (Particle Swarm Optimization), have been applied for zonation of the flood susceptible areas. The flood inventory dataset, prepared by satellite based collected flood samples, were apportioned into 70:30 classes to prepare training and validation datasets. One independent validation method, the Area-Under Receiver Operating Characteristic (AUROC) Curve, and other 11 cut-off-dependent model evaluation metrices have helped to conclude that the ANIFS-GA has outhustled other three models with highest success rate AUC = 0.922 and prediction rate AUC = 0.924. The accuracy was also found highest for ANFIS-GA during training (0.886) & validation (0.883). Better performance of ANIFS-GA than the individual models as well as some

ensemble models suggests and warrants further study in this topoclimatic environment using other classes of susceptibility models for the purpose of establishing a benchmark model with capability of highest accuracy and sensitivity performance in the similar topographic and climatic setting taking assumption of the quality of input parameters as constant.

Keyword: *Flood Susceptibility Mapping, ANFIS, Genetic Algorithm (GA), Differential Evolution (DE), Particle Swarm Optimization (PSO), metaheuristic optimization, Middle Ganga Plain*

1. Introduction

Floods, one of the most pervasive natural phenomena, are inflicting life, property (including livestock), soil loses (Keesstra et al., 2018), biodiversity losses (Keesstra et al., 2016)and ecological losses(Barredo, 2009; Cai et al., 2011; Yevjevich, 1994). Climate change induced flooding trend and pattern are increasing the complexity of this phenomena and related damages in the coastal areas is predicted to increase in the impending future (Hallegatte et al., 2013; Hanson et al., 2011). The flood related damages cannot be ignored and the complete prevention from it is unfeasible. It is this damage potential of floods that the United Nations has included this issue in its "United Nations Sustainable Development Goals (UNSDGs)" to properly tackle this menace and losses therefrom in a well-planned and strategic manner (UNSDG, 2013).The complex nature of floods, immensity of flood losses, and inclusion of flooding problem in the UNSDGs has made it essential and urgent to scientists to propose desirable and more accurate flood prediction methods for helping hazard management and mitigation agencies in better preparedness, planning for operational easiness, and make effective and adequate mitigation plans to curtail the damages from future flood events. The present flood modelling community is

attempting to develop and adopt more rigorous and logical mathematical approach to delineate the flood susceptible regions at different spatial scales including large and small scales. The approach inculcates various steps, some of the momentous ones are: preparation of inventory data with reasonable accuracy for training and validation purposes, the selection of most significant and high potential flood conditioning or geo-environmental factors which are suitable to tectonoclimatic and regional setting of the study area, digital elevation model (DEM) and satellite data with good spatial resolution to prepare the conditioning factor datasets, use of accurate & appropriate models, and assessment of the performance of models using advanced and reliable evaluation techniques. Among these steps, the step wherein the flood inventory data is prepared, utmost care of its accuracy must be taken into consideration because the training of models mostly depends on the quality of the inventory datasets; also, the accuracy of flood susceptible maps is compromised if the flood inventory data quality is not good(Khosravi et al., 2016a; Merz et al., 2007). The topography and hydro-climatological conditions influence the flood directly or indirectly, therefore, the selection of the flood controlling factors should also be done taking the type of topography under consideration. From an exhaustive literature survey and experts' knowledge of the field conditions, a list of common factors that are selected for spatial modelling have been prepared which includes altitude, aspect, slope, curvature, rainfall, soil, land use, land cover, stream density, distance to stream or rivers, distance to road, and topographic wetness index (TWI) (Arabameri et al., 2019e; Chapi et al., 2017a; Khosravi et al., 2016b; Sachdeva et al., 2017; Samanta et al., 2018; Tehrany et al., 2013). In recent studies the selection of additional factors is observed as normalized difference vegetation index (NDVI), topographic positional index, topographic ruggedness index (TRI), stream potential

index (SPI), and various other proxy factors that are prepared based on topography or/and hydro-climatology of the region. In hilly region, where the flash-floods are common occurrence, the nature of most important flood contributing factors' significance levels changes. In low altitudinal floodplain settings characterized by humid tropical to subtropical climate, geomorphology plays important role as compared to lithology. Whereas in mountainous watersheds, slopes and other factors play a relatively more significant role in flood occurrence potential prediction (Arora et al., 2019). Therefore, a caution should be practiced when selecting flood controlling factors for low altitude range viz. floodplain environment infested with conditions conducive to annual riverine floods and mere careless selection of flood control factors from the published literature irrespective of their topographic and climatic setting may cause diminished model performance. The study by Arora et. al. (2019) was conducted in the same area, by applying the level of caution as per the above suggestions, including a new control factor that is detailed microscale geomorphology, which has never been incorporated in previous studies of flood susceptibility prediction and had found that the geomorphology had not only played a better role than geology for flood susceptibility mapping for floodplains but its significance level was found to excel all other conditioning factors included in that study. In the earlier analysis, for the same study area, two models, one bivariate and one machine learning, were chosen and the prediction rates were found more than 80% for Frequency Ratio & Shannon's Entropy models. In present study, the geomorphology dataset has been upgraded and the previous geomorphology dataset was replaced by this new dataset with an aim to achieve different and better performance result.

The study area is the part of the Ganga river basin (GRB) where the monsoon induced heavy rainfall related annual flooding is a common phenomenon. The study area encompasses the confluences of major rivers flowing over the flood plain of GRB and also shares the state boundaries of Uttar Pradesh and Bihar. The majority of floods are reported by an international agency, Emergency database (EM-DAT), during 1985-2015 in states of Bihar, Uttar Pradesh, Assam, West Bengal, and Orissa in India (CRED, 2016). In most of the states where flood occurrences are very high, the prevailing topographic settings are conditioned with plain, low relief topography and lithological variability is minimal as the vast floodplains of the Ganga River and its tributaries are the source of sediment forming the lithological units, the prioritized selection of geomorphology over geology dataset appears to be logically strong and valid choice to test performance of various models of the flood susceptibility mapping (FSM) in such alluvial plain landscape. Again, whether the selected factors have interdependence on one another or have collinearity problem can be checked with multicollinearity analysis wherein the algorithm checks the collinearity among conditioning factors (Alin, 2010; Chen et al., 2018; Costache et al., 2020a). Afterwards, the relative importance of each factor can also be analyzed by different methods before applying models for spatial susceptibility prediction modelling; among them the frequently used methods are information gain method (Costache and Tien Bui, 2019; Đurić et al., 2019), Binary logistic regression (Arabameri et al., 2019b), Boosted regression tree (Arabameri et al., 2019f; Zabihi et al., 2019), and random forest model (Arabameri et al., 2019c). Under prevailing analysis the random forest model has been used to assess the competency of conditioning factors to fulfill the requirement for spatial modelling applications-based analysis. In order to achieve greater benefit from the conditioning factors, the selection of the satellite data or

other existing sources, data/maps, should also be of commendable quality to prepare these datasets. Among them, the hydrological and topographical based conditioning factor datasets are prepared through the remotely sensed imagery data and digital elevation model (DEM) data. A better spatial resolution remotely sensed satellite imageries also improve the quality of hydrological and topographical based conditioning factor datasets. Many studies have been including the ALOS PALSAR DEM dataset (Arabameri et al., 2019c), in place of lesser resolution shuttle radar thematic mapping (SRTM) DEM for preparation of topographic based conditioning factors. It may be noted that the ALOS PALSAR DEM the 12.5-meter spatial resolution dataset is freely available DEM data in public domain which is better than the SRTM DEM resolution of 30 meters for mountainous fluvial landscape studies (Boulton and Stokes, 2018). But in low altitude range environments SRTM 30m version 3 is vindicated to be widely acceptable in hydrological and landscape studies (Hayakawa et al., 2008; Zhang et al., 2019).

From last two decades, there have been continuous studies conducting FSM using different statistical techniques; it varies from bivariate statistical methods to multivariate models. The current trend in the natural hazard studies of large regions is focused on the use of machine learning (ML) (Achour and Pourghasemi, 2020; Häring et al., 2012; Hong et al., 2018b; Tehrany et al., 2015; Wang et al., 2020), multi-criteria decision making (MCDM),(Costache et al., 2020c; Oh et al., 2018; Santos et al., 2018) and ensembles models, combining two or more models, using bivariate, ML, and MCDM category models. There is no restriction on the selection of models for developing the ensembles; in other words, the selection of one model for creating the ensemble can be done from two or more different categories of models. It has also been observed in the flood modeling literature that the ensemble models

have performed more accurately than individual or standalone models (Bui et al., 2019; Chapi et al., 2017b; Choubin et al., 2019a; Shahabi et al., 2020). Among these published works, a study for FSM carried out by Chapi et al., (2017b)in Haraz watershed in northern Iran encompassing 4014 km^2study area shows that the combination of bagging ensemble with Logistic Model Tree (LMT) model has performed better than the LMT, logistic regression (LR), Bayesian logistic regression (BLR), and random forest(RF) standalone models. In another study ,Tehrany et al., (2015)had attempted Support Vector Machine (SVM) based ensembles prepared by using different kernel types to predict the flood susceptible regions, and their results demonstrated that SVM based ensembles have much better predication rate, >81%, than the standalone frequency ratio (FR) model. Recently, another class of hybrid model combining Adaptive Neuro Fuzzy Inference System (ANFIS) with Artificial Neural Network (ANN) and Fuzzy Logic models, has emerged to be frequently used for prediction of flood susceptible areas(Ahmadlou et al., 2019; Bui et al., 2018b; Hong et al., 2018b; Razavi Termeh et al., 2018). For instance, the study by Bui et al., (2018a) used ensembles combining the ANFIS with three metaheuristic models for FSM for a study area located in Iran and found that all three models have surpassed 94% prediction rate accuracy level. This study too, has vindicated the supremacy of ANFIS based ensembles compared to the standalones used in the study.

Benchmarking the flood susceptibility model, that is establishing the best performing most accurate and highly sensitive flood prediction model for a specific type of topoclimatic environment, keeping the quality of input parameters and model configuration settings constant, requires testing and validating all type of available models in each and every topoclimatic settings. It should be noted that there is considerable number of research work published in different parts of the world by

using the ANFIS based FSM, but to date, no such study applying this category of advanced novel flood ensemble models has been conducted for Ganga River Basin (GRB), India or in any part of India or in any part of the world with the such low altitudinal range topographic setting with characteristic climatic setting as MGP. In MGP, the southwest monsoon led heavy rainfall brings havoc every year, especially in lower basins of the GRB, and debouches heavy rainwater in the entire catchment and causes substantial amount of damages. Therefore, there is an immediate requirement in pursuit of benchmarking of flood susceptible models for this part of the Ganga river basin wherein some bivariate and machine learning individual models have already been tested and reported. This study is the next step in the pursuit of susceptibility model benchmarking in low relief sub-humid topoclimatic environmental setting and such study with other available highly advanced recent models must continue until the best model out of all the available models is achieved.

Keeping in view the research gaps and orientation of research of flood susceptibility modeling community, the aim of this study has been set to assess and analyze the performance of novel advanced models, ANFIS (standalone) and three of its hybrids optimized with Genetic Algorithm (GA), Differential Evolution (DE), and Particle Swarm Optimization (PSO) viz. ANFIS-GA, ANFIS-DE, ANFIS-PSO, for prediction of flood susceptible zones in the MGP. The novelties of this study lie in the first time use of ANFIS and three of its advanced ensembles for FSM and evaluation of the different aspect of models' performances through the use of a hot of cut-off-dependent &cut -off-independent matrices.

2. Description of the study area

The Middle Ganga Plain (MGP) is the most densely populated part of the of the Ganga River Basin (GRB)(Singh, 1971).And, the present study area holds the densest populated region of MGP. The study area shares the most densely populous districts, Patna, Siwan, Saran, Vaishali, Samastipur, Begusarai, Nalanda, and Bhojpur of Bihar state. Geographically, the study area extends between 25°10′N-26°10′N and 83°90′-85°45′E latitudes and longitudes. It accounts for a total of 10,138 km^2area of upper and lower GRBs. The MGP witnesses floods almost every year during monsoon and even the post-monsoon seasons do not remain dry and cause flooding under the influence of the South-West monsoon rainfall (Vittal et al., 2016). In the MGP, there are confluence points for five major rivers and their tributaries viz. Ganga, Gandak, Ghaghara, Kosi, and Son (Arora et al., 2019). Therefore, such vast upper catchment area with latitudinal climatic and topographic gradient enhances the proneness of these low lying floodplains, having major confluence zones of big rivers, to severe flooding every year during both monsoon as well as post-monsoon periods.

The region experiences summer (April–May), monsoon (June–September), post-monsoon (October–December) and winter (January to March) seasons in a year (Dimri et al., 2019). Due to sub-tropical-humid climate the MGP observes the highest temperature during the months from April to July. It ranges between 35 to 45°C during summer season. The lowest temperature 3-4°C is observed during the months of December and January. The southwest monsoon hits the MGP during sometime between late June and early July. The high intensity rainfall in the upper catchments of GRB causes floods in the MGP in post monsoon season, also, during the months of August and September. The in-situ water discharge data, for Gandhighat station, Patna, obtained from Central Water Commission (CWC), Govt.

of India, reveals that the maximum average monthly water discharge is recorded during the months of August & September which result into the post monsoon flooding in the MGP. From the collected water discharge data, it has been observed that the average annual discharge for Gandhighat station soars up to 50,000m^3/sec in a single day, during the flood months. The high water discharge in the streams increases the possibility of levee breaches and bank overflow resulting into flooding. The location map of CMGM overlapped with district-wise no. of household and the recorded average monthly discharge of Ganga river at Gandhighat station during monsoon period (June to October) for year 2008 is demonstrated in figure 1.

3. Materials and methods

3.1 Data used

3.1.1 Flood inventory data

The flood inventory data should be prepared with accuracy before using it for extracting random sample points to be later used of model training and validation in the studies related to flood (Choubin et al., 2019b), whereas, precision in the sample point collection process increase model accuracy for prediction (Arora et al., 2019; Tehrany et al., 2013). For generation of accurate flood inventory, the Landsat satellite data, series 5, has been downloaded from the Earth explorer website (https://earthexplorer.usgs.gov/) for the pre-flood, during-flood, and post-flood periods. The details of the downloaded datasets are provided in table 1. The complete exercise of preprocessing of satellite imageries and retrieval of inundated pixels using Normalized Difference Water Index (NDWI) has been already explained by Arora et al. (2019).

In present work, we have generated a total 1000 random floodpoints and the same number of non-inundation points have been also generated. Out of which, 70% have been utilized for training and remaining 30% have used for testing purposes.

3.1.2 Conditioning factors (CgFs)

The construction of CgFs datasets was accomplished by using the SRTM 1-arc sec (30m) DEM along with re-analysed meteorological data, and some existing streatmaps. The DEM generated CgFs are Altitude, Curvature, Distance from streams, Stream density, Slope (degree), Slope Aspect, and TWI. The Land Use Land Cover (LULC) map for the year of 2008 was downloaded from the European Space Agency (ESA) led Climate Change Initiative (CCI) (https://www.esa-landcover-cci.org/). The ESA has archives of generated annual LULC data for the period 1992-2015 at global scale at 300m resolution and provides the same on their web portal for utilization in studies related to non-commercial purposes(Li et al., 2018).The soil data was procured from the Food and Agriculture Organization (http://www.fao.org) of the United Nations. The geomorphology data was procured in vector format from the Bhukosh Portal of the Geological Survey of India website (http://bhukosh.gsi.gov.in/Bhukosh/Public). The rainfall data was prepared by the retrieved data from Climate Forecast System Reanalysis (CFSR) web-portal (https://globalweather.tamu.edu/). The distance to road data was prepared by using the downloaded road network from Open Street Map portal (https://www.openstreetmap.org/).Thereafter, to achieve the homogeneity, all collected data was converted into raster format and resampled at 30-meter resolution to use further for spatial modelling.

The altitude range in the study area is so low (13 -96 m) that it appears almost homogenously featureless topographic setting when viewed in medium resolution dataset. This is the reason why the vast floodplains of GRB have long been considered featureless (Singh, 1971) and still there is no geomorphological maps at finer scales like 1:25000 or 1:5000. The altitude dataset is demonstrated with training and validation sample points in figure 3A.

Due to plain topography, the plan curvature in most parts of the MGP is flat type. The convex and concave types of curvature can mainly be found along river banks or along major topographic break points like terraces etc. (figure 3B)

The figure 3C & figure 3D are showing the distance to road & distance from stream datasets, respectively. Both of the datasets have been prepared using Euclidean distance analysis method. The maximum distance of 7073 meters was noted for the road network and 5383 meters for the stream network from their respective connected points. The equation (1) of Euclidean distance method is mathematically expressed as follows:

$$d(x,y) = \sqrt{\sum_{i=1}^{n}(x_i - y_i)^2} \quad (1)$$

Where *x* and *y* are two points in Euclidean n-space and *d* refer distance between *x* and *y.*

The geomorphology map of the MGP is displayed in figure 3E. The geomorphology dataset is combined form of 21 geomorphological units; each unit plays a significant role in flood prediction potential. The most important unit is the FluOri- active flood plain unit where the probability of the flood occurrences is very high. The detailed information of each unit is provided in the table 2.

LULC is the mosaic of all the natural and man-made features; both categories, of the earth surface, have influence over hydro-meteorological processes, directly and indirectly. The LULC map (figure 3F) is categorised into four categories- Agricultural Lands, Vegetation/Treecover, Built-up Lands, and Water Body (Rivers/Ponds).The maximum number of flood sample point is observed to be in agricultural lands class of LULC.

The rainfall dataset prepared using the interpolation analysis of collected CFSR data for ~36 years (Jan 1979-Jul 2014). The numerical average data for all stations were assembled before running the Inverse Distance Weighted (IDW) interpolation algorithm (equation 2). The IDW is widely used in earth sciences related studies (Bartier and Keller, 1996). The prepared rainfall map, displayed in figure 3G, provides the spatial overview of rainfall distribution. The highest average annual rainfall was recorded 1281mm for MGP whereas the lowest value was noted to be 1002mm only. The highest rainfall is observed in south-west and south-east parts of MGP represented by dark blue in the displayed map.

$$Z_{x,y} = \frac{\sum_{i=1}^{n} z_i w_i}{\sum_{i=1}^{n} w_i} \qquad (2)$$

Where $Z_{x,y}$ refers to the point value (rainfall) to be estimated, z_i represents control value for i_{th} sample point, and w_i is a weight that determines the relative importance of individual control point z_i during interpolation process.

Slope aspect indirectly influence the floods through employing control on various geo-environmental factors i.e. soils, vegetation, rainfall, etc. (Rahmati et al., 2016). The slope aspect map (figure 3H) has been categorized in nine divisions ranging

337 from flat to Northwest zones. The following equation (3) was used to calculate the
338 slope aspect:

339 $$Aspect = 270° + arctan\left(\frac{f_y}{f_x}\right) - 90° \frac{f_x}{|f_y|°} \quad (3)$$

340 Where, f_x and f_y are the rate of change in latitude values measured in the north-south
341 and the east-west directions, respectively (Hu, 2016).

342 The slope of a region controls and influences the hydrological activities; affects the
343 surface directly (Tehrany et al., 2019). Due to the plain topography a very low
344 variance in the slope for MGP existed. The slope map (figure 3I) provides the
345 detailed visualization of slope (in degree) for the study are.

346 In MGP, total six soil types are found as shown in soil map (figure 3J) of MGP.
347 Among all six categories of soils, the maximum spatial coverage is observed by the
348 FL-Fluvisols (3743) category. The FL-Fluvisols category covers the active floodplain
349 mostly as well as it covers the maximum share of flood samples.

350 Per unit area of the total length of all stream networks is called the stream density or
351 drainage density (Sangireddy et al., 2016).The probability of flood occurrences is
352 very high at high stream density places (Onuşluel Gül, 2013). The stream density
353 map (figure 3K) prepared by using the line density tool of ArcGIS toolbox. The
354 maximum and minimum density was recorded 75.60 km/km^2& 0.96
355 km/km^{2}respectively.

356 The TWI is calculated by dividing the specific basin area by the slope of the region.
357 The TWI map is displayed in figure 3L. The mathematical representation, equation
358 (4), of TWI calculation is as follows:

$$TWI = \ln\left(\frac{A_s}{\beta}\right) \quad (4)$$

Where $A_s$represents the particular catchment area and βindicates slope angle.

3.2 Methodology

The flowchart of methodology is provided in figure 2. The following section would provide a brief detail of models used in this study.

3.2.1 Description of models

3.2.1.1 Multi-Collinearity Analysis

The multicollinearity analysis (MCA) helps to find collinearity among conditioning factors (CgFs), if present, and allow a user to decide the non-collinear CgFs for further analysis in order to get unbiased results by spatial modelling. Hence, the MCA is recommended for a spatial modelling study (Arora et al., 2019). The published research works suggest use of two indices, Variance Inflation Factor (VIF) and Tolerance (TOL) under MCA to evaluate collinearity dependency of CgFs among each other and, subsequently, the CgFs found suitable for further analysis if the TOL >0.1 & VIF<10 retrieved in results (Hair et al., 2013; Menard, 2002).

These two indices, TOL and VIF, can be calculated by the following equations:

$$TOL = 1 - R_{\mathrm{v}}^2 \quad (5)$$

$$VIF = \frac{1}{TOL} \quad (6)$$

Where R_{v}^2 represents the ‘coefficient of CgFs on all other CgFs’

3.3.2 Determination of relative weights for conditioning factors

379 The Random Forest (RF) model is an ensemble-based learning algorithm where a
380 large pool of decision-trees (DTs) are constructed to perform the spatial relationships
381 between an event (occurrence of flood) and the related factors (CgFs) for
382 classification (Lee et al., 2017). A pair of decision trees analyses the classification
383 (also refers as 'vote' in model) and the maximum number of votes by the class
384 concluded as the results of RF (Arabameri et al., 2019d). The determination of each
385 factor is decided by the importance of used variables in the model. In comparison to
386 other decision tree methods the results generated by RF model found with less
387 errors due to the use of multitude set of trees. At this instance, the RF model has
388 been used to determine the relative weights or importance of each CgFs.

389 The flood conditioning datasets $FCD = (x_i, y_i)_{i=1}^{N}$ with $x_i \in R^M$ is the CgFs; where '*N*'
390 refers the total number of samples and *'M'* is the total count of CgFs. $y_i \in (1,0)$ is the
391 output which contains flood (1) & non-flood (0) occurrences. In first step, the
392 bootstrap algorithm used to generate *n* subsets (bootstrap subsets), where each
393 subset consists of *'m'* factors; where $m \leq M$. Then, in second step, the CART
394 (Classification And Regression Tree) algorithm has been used to construct the tree
395 classifier for each bootstrap subset (Arabameri et al., 2019f). In final stage, all
396 constructed classifiers have been aggregated to design a RF classifier. In general, to
397 construct a RF model, two parameters: *'n'* & *'m'* should be determined, where *'n'*
398 should be large enough, i.e. 'n'= 500 (Tien Bui et al., 2016) to contrast the RF model.
399 The total number of variables was restricted to 3 at each split of the model and the
400 Out-of-bag (OOB) estimate of error rate was found 30.34% for the performed model.

401 3.3.3 Flood susceptibility mapping (FSM)

The FSM has been conducted in the study through four models are- ANFIS and ensembles with GA, DE, & PSO heuristic models. Brief information of all four models has been provided in following sub-sections.

3.3.3.1 Adaptive neuro-fuzzy inference system (ANFIS)

The neuro-fuzzy network, ANFIS, was proposed in 1993 (Jang, 1993)and since then is being used in different disciplines of sciences including geosciences (Ahmadlou et al., 2019; Lei et al., 2007; Naderloo et al., 2012; Najafi and Faizollahzadeh Ardabili, 2018; Razavi Termeh et al., 2018; Republic, n.d.; Wei et al., 2007). The output of this adaptive network depends upon the parameters of nodes and to optimize the performance during training of the parameters there are two kinds of learning algorithm applied to tune these parameters (Li and Su, 2010). In other words, the system of ANFIS can be understand as there are two inputs, x & y, and an output z. There are five layers or steps, presented by if-then fuzzy rules, based on Sugeno model, to calculate the output (Takagi and Sugeno, 1985).

$$Rule\ 1: if\ x\ is\ A_1\ and\ y\ is\ B_1, then\ f_1 = p_1x + q_1y + r_1 \quad (7)$$

$$Rule\ 2: if\ x\ is\ A_2\ and\ y\ is\ B_2, then\ f_2 = p_2x + q_2y + r_2 \quad (8)$$

Where the fuzzy sets are A_1, A_2, B_1, and $B_2$and the modifiable parameters are represented by$p_i, q_i, \text{and} r_i$; $f_i$indicates separated outputs for both rules.

Layer 1: every node I is an adaptive node with node function

$$O_i^1 = \mu A_i(x), i = 1,2 \quad (9)$$

$$or$$

$$O_i^1 = \mu B_{i-2}(y), i = 3,4 \quad (10)$$

Where x (or y) is the input to the node *i* and A_i (or B_{i-2}) represents linguistic label associated with node.O_i^1 or O_i^1 are the membership function for A_i (or B_{i-2}), specifies the degree where the given *x or y* satisfies A_i or B_{i-2}. The *A* and *B,* the membership functions, usually denote as bell functions (Übeyli et al., 2010):

Generally,$\mu A_i(x)$ is chosen to be bell-shaped with maximum and minimum equal to 1 and equal to 0 respectively, such as

$$\mu A_i(x) = \frac{1}{1+\left|\frac{x-r_i}{p_i}\right|^{2q_i}} \quad (11)$$

where {p_i, q_i, r_i} are called premise parameters.

Any continuous and piece-wise distinguishable function, like a triangular-shaped membership function, is also a qualified member for the node function in this layer (Catalão et al., 2011). The parameters in this layer are noted as premise parameters.

Layer 2: Every node is a fixed node, represents the firing strength of the rule, in this layer, and acts multiplies the incoming signals/parameters. The output represents as;

$$O_i^2 = w_i = \mu A_i(x) \times \mu B_i(y), \ i = 1,2 \quad (12)$$

Layer 3: In this layer, each node refers an adaptive node labelled as 'N', computes the ratio of the i_{th} rule's firing strength to the sum of all rules' firing strengths:

$$O_i^3 = \overline{w}_i = \frac{w_i}{w_1+w_2}, \qquad i = 1,2 \quad (13)$$

Generally, the outputs are labelled as normalized firing strengths.

Layer 4: In this layer, each node called an adaptive node, computes the contribution of the i_{th} rule to the overall output, with a function:

$$O_i^4 = \bar{w}_i z_i = \bar{w}_i(a_i x + b_i y + c_i), \qquad i = 1,2 \tag{14}$$

Where, $\bar{w}_i$indicates the output of layer 3, and $(a_i, b_i, c_i)$are the parameter set; also referred as consequent parameters.

Layer 5: In final layer or layer 5, the single node or fixed node calculates the overall output by summing all incoming/retrieved signals from preceding ones:

$$O_i^5 = \sum_i \bar{w}_i z_i = \frac{\sum_i w_i z_i}{\sum_i w_i} \qquad i = 1,2 \tag{15}$$

3.3.3.2 Genetic algorithm (GA)

The GA was first proposed in 1989 (Booker et al., 1989) by inspiring from the Charles Darwin's theory: 'survival of the fittest' (McCall, 2005). The basic concept behind the robust GA is to perform natural selection test, even in noisy environments. The algorithm discovers the best output or solution among resultant outputs in three steps- 'Selection', 'Crossover, and 'Mutation'.

In each step, the algorithm randomly selects and analyse individuals from the population and further utilize them to produce the new data or children for the next generation and it repeats until retrieve the ideal result(Li and Su, 2010).

3.3.3.3 Differential evolution (DE) algorithm

The DE, a stochastic, population-based optimisation and an evolutionary algorithm developed to finding a solution (Price et al., 2006; Storn, 1999). Here, a brief detail of

the algorithm is explained, the complete details may read elsewhere (Storn and Price, 1995). The algorithm performed in four steps, Initiation, Mutation, Crossover, and Selection, to solve a complex problem.

Initiation: In initiation, the initial population, N_p size, randomly generated; where, the decision parameters for each values are assigned (Tien Bui et al., 2017).

$$X_{j,i} = X_j^{min} + m_j(X_j^{max} - X_j^{min}) \quad (16)$$

Where *i =1, 2,…., N_p* and *j =1, 2,….,D;* [*D* indicates decision variables number].X_j^{max} is upper bound while X_j^{min} is indicating the lower bounds of the decision j^{th} ; and 'm' is a random number in '0' to '1' range.

Mutation: The mutation operator generates mutated or differential (donor) vectors in which each vector constructed by following rule;

$$X_{j,gen+1} = X_{r_{1,gen}} + F(X_{r_{2,gen}} - X_{r_{3,gen}}) \quad (17)$$

where*r1, r2,* and *r3* are randomly chosen indices [*r1 ≠ r2 ≠ r3 ≠ i*]; $X_{r_{1,gen}}$,$X_{r_{2,gen}}$, and $X_{r_{3,gen}}$are randomly selected valued from the populations, and *F* is the scale factor.

Crossover: This operator used donor & target vectors to produce a trial vector(Hong et al., 2018a);

$$X'_{j,i,gen+1} = \begin{cases} X_{j,i,gen+1} \text{if } \rho_j \le C_R or\ j = q \\ X_{j,i,gen} \quad else \end{cases} \quad (18)$$

Where $\rho_j \in [0, 1]$ is a uniform random number, $C_R \in [0, 1]$ represents the crossover parameter, and $q \in \{1,..., D\}$ represents as an index as assurance for selection of one of the parameter, at least, in the mutant vector.

Selection: In comparison of fitness value of trial vector with target vector, the selection operation is used to choose the best choice for the next generation;

$$X_{i,gen+1} = \begin{cases} X'_{i,gen+1} \text{if } f(X'_{i,gen+1}) \leq f(X_{i,gen}) \\ X_{i,gen} \quad else \end{cases} \tag{19}$$

Where, $X_{i,gen}$represents parent vector, and *f (*)* is called the fitness function.

3.3.3.4 Particle swarm optimization (PSO) algorithm

The swarm intelligence, inspired by the shared behaviours of animal was used to find out the distributed solutions (Chen et al., 2020). The PSO algorithm, based on swarm intelligence, was developed by Kennedy and Eberhart, (1995)to know the social behaviour of birds flock and their food catching processes. In some aspects, PSO can be referred as an evolutionary method such as GA. But in PSO the genetic operation is unavailable, which is used to produce a next generation solution in GA. In PSO algorithm, a random number of feasible solutions, described by vectors, generated at the time of initialization of it to find the optimal solution (Mehrabi et al., 2020). The solution in PSO is also referred as particle. In order to evaluated the potential of each particle, the velocity has been assigned to each one of them, who have been positioned randomly, by calculating the fitness value (p_{best}) and the elite position (g_{best}) of each particle (Moayedi et al., 2020). The PSO algorithm process can be expressed mathematically as;

$$N'_i = wN_i + C_1 r_1 (p_{best} - R_i) + C_2 r_2 (g_{best} - R_i) \tag{20}$$

$$R'_i = R_i + N'_i, \tag{21}$$

The computation to change the velocity (R_i) of each particle toward the location of the identified p_{best} and g_{best}.

Where,N_i represents the particle position; $C_1$and C_2represent the cognitive and social scaling parameters respectively, andR_i is the velocity of each particle. The $r_1$and $r_2$symbolize the random numbers between 0 and 1 and *w* is the inertia weight.

3.4 Evaluation and Comparison of models

The performance assessment of involved models has been completed by two methods: cut-off-independent and cut-off-dependent methods. The receiver operating characteristics (ROC) as a cut-off-independent evaluation method is found most reliable and successful robust technique to assess the model performance (Arora et al., 2019; Schumann et al., 2014). Whereas, the dependent matrices evaluation methods, i.e. accuracy, F-score, sensitivity, specificity, odd ratio, and Cohen's Kappa, etc., have been utilized to assess the model performance along with ROC to have evaluation of different facets of model performances. The precise model evaluation requires both dependent and independent matrices evaluation methods (Rahmati et al., 2019). Rahmati et al. (2019) have reviewed 21 cut-off-dependent metrices and have defined clearly what those metrices refer to. These different cut-off-indices may be of use to end user agencies interested different aspects of the model performance. For example, if the end user agency expresses desire to know a model's ability to incorrectly predict non-flood events, it will directly look on that models, FPR (or fall out) which equals '1-specificity). Similarly, if the agencies' need is to know overall error rate, it will look into the 'misclassification rate' column of cut-off-dependent indices table.

In order to calculate the results based on above discussed evaluation methods, the confusion matrix for training and validation datasets for flood modelling in 2 × 2 row and column format table is prepared. Where, four types of possible consequences,

including true positive (TP), false positive (FP), true negative (TN), and true positive (TP), occurrences were analysed. The TP indicates the correctly classified pixels of flood event; FP is representing the count of incorrectly classified pixels as flood event. Whereas, the correctly classified pixel as non-flood is called TN and FN describes the number of incorrectly pixels classified as non-flood. Based on these four possible consequences, TP, FP, TN, & FN, the specificity, true positive rate (TPR), sensitivity, false positive rate (FPR), false discovery rate (FDR), false negative rate (FNR), accuracy, precision, F-Score, accuracy, odd ratio and Cohen's kappa statistics are calculated and equations of these metrics are as follows:

$$TPR = Sensitivity = \frac{TP}{(TP+FN)} \quad (22)$$

$$Specificity = \frac{TN}{(TN+FP)} \quad (23)$$

$$FPR = \frac{FP}{(TN+FP)} = (1 - Specificity) \quad (24)$$

$$FDR = \frac{FP}{(TP+FP)} \quad (25)$$

$$FPR = \frac{FP}{(FN+TP)} \quad (26)$$

$$Accuracy = \frac{TP+TN}{(TP+TN+FN+FP)} \quad (27)$$

$$Precision = \frac{TP}{TP+FP} \quad (28)$$

$$F - Score\ (F_\beta) = \frac{(1+\beta^2)(Precision \times Sensitivity)}{(\beta^2) \times (Precision+Sensitivity} \quad (29)$$

553 Where, β, a default parameter, is commonly 0.5,1 or 2; in the present study, β = 1 is
554 being taken.

555 The odd ratio analysis checks odds of occurrence of an event due to presence of a
556 particular factor (or exposure as called by Pepe et al., 2005)as compared the odds of
557 occurrence of that event in the absence of the same exposure(Pepe et al., 2005).

558 $$Odd\ Ratio = \frac{(\frac{TP}{FP})}{(\frac{TN}{FN})}$$

559 (30)

560 The Kappa statistics is a measurement of agreement between two distinguished sets
561 of classification while catering the randomness in the classification (Arabameri et al.,
562 2020a). The Kappa statistics can be computed with the equation which isas follow:

563 $$K = \frac{P_{obs} - P_{exp}}{1 - P_{exp}}$$ (31)

564 Where, P_{obs} is observed agreements = (TP+TN), represents the correctly classified
565 values of inundated and non-inundated pixels.

566 P_{exp} is expected agreements = [{(TP+FN) x (TP+FP)} + {(FP+TN) x
567 (FN+TN)}]denotes the proportion of inundated and non-inundated pixels which were
568 expected to show agreement, on the basis of chance (Hoehler, 2000).

569 The value of K ranges between 0 and 1, where the lower value, towards '0', indicates
570 less agreement and higher values, towards '1', shows higher or near to perfect
571 prediction. The various range of K indicates different agreement i.e., K ≤ 0 (no
572 agreement); 0.01 - 0.20 (slight agreement); 0.21 - 0.40 (fair agreement); 0.41- 0.60
573 (moderate agreement); 0.61- 0.80 (substantial agreement), and 0.81 - 1.00 near to
574 perfect agreement (Cohen, 1960) .

The area under the ROC (AUROC) curve measurement describes the evaluated prediction value ranges from 0.5 to 1.0, inaccurate to highly accurate (Marzban, 2004). In this method, the FPR and TPR are plotted on the x-axis and y-axis, respectively. The AUROC values can be classified to measure the accuracy into following four descending order classes: excellent (0.9–1.0), good (0.8–0.9), fair (0.7 to 0.8), and poor (0.6 to 0.7) (Fressard et al., 2014). The AUROC can be calculated as follows(Chapi et al., 2017b):

$$AUCROC = \sum TP + \sum TN/P + N \quad (32)$$

In order to check the errors in the models, the Root Mean Square Error (RMSE) test has been conducted. The RMSE is a standard statistical metric to assess a model's performance in various subjects of sciences(Chai and Draxler, 2014). The RMSE can be explained mathematically;

$$RMSE = \sqrt{\frac{\sum_{i=1}^{n}(P_i - O_i)^2}{n}} \quad (33)$$

Where the P represents the predicted cases, O refers as observed values, and n is the total number of cases.

In order to check the classification accuracy of the models, the seed cell area index (SCAI) method has been used. The index calculation can be achieved through the ratio of each classified class and the susceptible seed cell percent values (Süzen and Doyuran, 2004).

$$SCAI(\%) = \frac{\frac{N_{pix}(X_j)}{\sum_{j=1}^{n} N_{pix}(X_j)}\ (area\ ratio) \times 100}{\frac{N_{pix}(SX_i)}{\sum_{i=1}^{m} SX_i}\ (flood\ susceptible\ occurance\ ratio) \times 100} \quad (34)$$

Where $N_{pix}(SX_i)$ is the number of pixels with flood occurrence cases within class *i* of factor variable *X*, $N_{pix}(X_j)$refers the number of pixels within the factor variable X_j, *m* indicates the number of classes in the parameter variable X_i, and *n* represents the number of factors in the study area.

If the low SCAI value fall low for the 'high' and 'very high' susceptibility classes and high SCAI values represent the 'low' and 'very low' flood susceptible classes, fora model results, then the model output classification is said to be for that model (Arabameri et al., 2020b).

4. Results and analysis

4.1. Independent analysis of the conditioning factors

The result of MCA for all 12 flood CgFs is presented in table 3. The analysis shows that the TOL values of all 12 CgFs factors are less than 1.0 and the VIF for the same CgFs has been found to be less than 1.9, which suggests that there is no collinearity issue among all 12 CgFs. Therefore, all the factors were further utilized for FSM for prediction.

4.2 Relative weights of conditioning factors

The RF model-based importance of all flood CgFs with their corresponding ranks are presented in table 5. The higher value of a conditioning factor shows their higher importance in FSM (Arabameri et al., 2019f). The results revealed that the highest

predictability in the list of all twelve CgFs, for flood is secured by the geomorphology (0.130). The other major predictors which follow geomorphology, in order of their diminishing importance, are: distance to streams (0.121), curvature (0.103), slope (0.099), stream density (0.094), and LULC (0.082). The other CgFs who play moderate roles in predictability are TWI (0.072), distance to road (0.071), slope aspect (0.070), and altitude (0.070). Two least important predictors are soil (0.050), & rainfall (0.038).

The retrieved values (significance score) and ranking by RF model for all CgFs have been further utilized in prediction of flood using all four models.

4.3 Results of models

The results of all four model-based flood susceptibility models categorized in 5 flood potential classes: very low, low, moderate, high, & very high are displayed in figure 4 (ANFIS), figure 5 (ANFIS-GA), figure 6 (ANFIS-DE), and figure 7 (ANFIS-PSO). For the purpose of presenting the clear picturisation of flood susceptibility near confluence zone, two highly flood susceptible windows have been zoomed-in in all the four maps. All the model results are classified using natural break (NB) method and the class-wise distribution statistics of all the classified map results using NB method is also displayed in the figure 8. In order to have more deeper insights of class-wise areal distribution for each model, the percentage of high & very high classes obtained through different classification methods/schemes viz. Quantile (QNTL), NB, Geometric Interval (GI), & Equal Interval (EI) have also been portrayed in figure 9.

The FSM-ANFIS derived flood susceptibility prediction index (FSPI) values range from 0 to 0.077 which has been divided into five categories using NB method. The

643 very low (0-0.077) class occupies about 32% of area while ‘low’ class (0.078 to 0.24)
644 covers around 40.58% of area in MGP region. The ‘moderate class’ FSPI ranges
645 from 0.25 to 0.43 and represents 10.40% of area. The least area coverage (about
646 4.8%) representor is the ‘high class’ (0.44-0.65). And, the ‘very-high class’ (FSPI
647 range: 0.66 -0.779) falls into 12.27% of total region.

648 The FSM-ANFIS-GA values have also been segmented (using NB) into five classes.
649 The ‘very low-class’ values ranging from 0-0.21, are distributed mainly in higher
650 lands of the basin, occupying 22.49% area. The second category, ‘low class’ values
651 ranging between 0.22 and 0.34, cover 26.15% of the total classified region. About
652 17.53% of the area is covered by ‘moderate class’ (FSPI range: 0.35-0.49) that
653 mostly occupies the outer parts of the river basin. The fourth class in the list is the
654 high potential range between 0.5 and 0.66 covering 14.53% while the ‘very high’
655 (FSPI range: 0.67 to 0.99) flood potential category for ANFIS-GA occupies the
656 second highest share, 18.90%, among all incorporated four models.

657 The values for FSM-ANFIS-DE model-based map range between 0.02 and 0.99; and
658 has been partitioned into five groups using NB. The very low (0.02-0.24) flood
659 potential has spread over 25.06% of the total area in MGP. The highest area of
660 25.41% has covered by the second category ranging between 0.25 and 0.38. The
661 moderate values range from 0.39 and 0.54 and occupy 22.73% of the total area. The
662 maximum share of 17.29% of the total area of high flood potential values (0.55-0.71)
663 has been predicted by ANFIS-DE among all models. About 9.5% of total area has
664 been claimed by very high (0.72-0.99) flood potential class.

665 The values of FSM-ANFIS-PSO are included in the interval between 0.06 and 0.94
666 partitioned into five classes using NB method. The first category, very low values

667 range between 0.06-0.23 and are distributed mainly in older floodplain of MGP
668 covering 22.82% of the total area. The highest share, 25.48% of the total area, has
669 been covered by the low category ranging from 0.24 to 0.35, expanding mostly in the
670 central part of MGP along with Ganga River. The third category, moderate class,
671 ranging between 0.36 and 0.50, occupies 16.67% of the total area. About 14% of
672 area has been predicted under the 'high category' (0.51-0.66) by the ANFIS-PSO
673 model. The 'very high' class values ranging between 0.67 and 0.94, secured the top
674 position in terms of predicting the flood potential in MGP with 20.77% of the total
675 area.

676 The results show that the maximum share of very high class having highest
677 probability of flood occurrences, is predicted by ANFIS-PSO (20.77%) followed by
678 ANFIS-GA (18.90%), ANFIS (12.27%), and ANFIS-DE (9.52%). If examined from
679 another scenario, after merging both the high & very high categories, the maximum
680 share of flooded areas has been secured by ANFIS-PSO (35.03%), ANFIS-GA
681 (33.42%), ANFIS-DE (26.81%), and ANFIS (17.08%). Hence, it can be observed that
682 the ANFIS-PSO has secured the prime position in terms of predicting most high &
683 very high categories of flood occurrences.

684 In order to compare the results of classifications, another analysis has been done
685 wherein the class-wise distributions of all four models using QNTL, NB, GI, and EI
686 classification schemes, it is found that the ANFIS-PSO & ANFIS-GA have shown
687 better performance than other two models in terms of predictability of the ';high &
688 very high classes' of flood susceptible lands. The ANFIS model has found to be the
689 least performant in terms of sharing the high class using NB (4.81%) and EI (5.26%)
690 classification schemes whereas, ANFIS-DE model has been found to be at the end
691 of the list for sharing the very high class using EI (5.78%) and NB (9.52%).

4.4 Evaluation of the FSM

4.4.1 Cut-off-independent evaluation metric: AUCROC

The AUC evaluates the overall performance of a model (Jaafari et al., 2019; Khosravi et al., 2019; Liu and Li, 2005; Pham et al., 2019). In the present study, a promising and acceptable level of AUC was found in the case of all four models ~~in~~ both with respect to training (success rate) and validation (prediction rate). The AUC_{SR} (success rate AUC) ranges between 0.807 and 0.922 whereas the AUC_{PR} (prediction rate AUC) was found between 0.768 and 0.924 for ANFIS model and its three ensembles. The highest position for success (AUC = 0.922) and prediction (AUC = 0.924) was secured by ANFIS-GA. The ANFIS-PSO positioned at second in the list with AUC=0.915 (success) and AUC = 0.921 (prediction). Among the other remaining two models, ANFIS (AUC_{SR} = 0.807; AUC_{PR}=0.768) & ANFIS-DE (AUC_{SR} = 0.901; AUC_{PR}=0.919), the latter had been found to be more accurate than the former in terms of training & testing accuracy. The success rate curve (SRC) and prediction rate curves (PRC) are shown in Figures 10A and 10 B, respectively.

4.4.2 Cut-off-dependent evaluation matrices

In order to calculate the cut-off-dependent matrices, the collected True Positive (TP), False Positive (FP), True Negative (TN), and False Negative (FN) samples were utilized. The complete results are provided in table 6.

4.4.2.1 Accuracy (Ac)

The first in the list of dependent evaluation matrices is accuracy, which defines that how accurately the model has performed during training and validation of the data. This metric's values range between 0 and 1; the higher value indicates more

accuracy and the vice versa. The maximum accuracy has been observed for ANFIS-GA for training (0.886) and validation (0.883), followed by ANFIS-PSO with accuracy levels of 0.871 for training and 0.875 for validation whereas the lowest accuracy was seen in case of ANFIS model with accuracy values of 0.855 for training and 0.853 for validation.

4.4.2.2 Sensitivity (Sn)

The Sn is calculated by dividing the number of true positive predictions by the total positive values (sum of true positive & false negative values). The highest sensitivity was recorded during training of the model for ANFIS-GA (0.886) followed by ANFIS-PSO, ANFIS-DE (0.867), and ANFIS (0.863). During validation process, the ANFIS-GA & ANFIS-PSO shared the first position with sensitivity figure of 0.867. The second position was secured by ANFIS-DE (0.858) and in the last position; the ANFIS (0.847) has been placed.

4.4.2.3 Specificity (Sp)

The Sp is calculated by dividing the total number of true negative predictions by the total negative counts (sum of false positive & true negative values). The specificity also refers as precision of the model. The prime position during training of model was secured by ANFIS-GA (0.887) following with ANFIS-PSO (0.876), ANFIS-DE (0.869) and ANFIS (0.847). Again, during validation, the ANFIS-GA (0.900) outhustled the other three models; ANFIS-PSO (0.883), ANFIS-DE (0.867) and ANFIS (0.860).

4.4.2.4 F-Score

In order to provide more insights about performance comparison using dependent evaluation metrices for each model, the F-score is also computed in the study; it analyses the harmonic mean score through the calculated precision and sensitivity of the data (Rahmati et al., 2019). The ANFIS-GA has received the highest F-Score during training (0.886) and validation (0.881). The ANFIS-PSO has also performed better in comparison to other two models and had scored very well during training (0.871) and validation (0.874). The third position was secured by ANFIS-DE during training (0.868) and validation (0.861). The least performant was ANFIS which was found positioned at the last in the list during training (0.856) and validation (0.852) procedures.

4.4.2.5 Cohen's Kappa (K)

By analysing the K-metric of all the models during training and validation, it was found that the consistent performing model was ANFIS-GA. During training, the top rank was secured by ANFIS-GA (0.773); with the following successors: ANFIS-PSO (0.743), ANFIS-DE (0.736) and ANFIS (0.710). The ANFIS-GA secured the first place with K = 0.767 during validation followed by ANFIS-PSO (0.750), ANFIS-DE (0.723), and ANFIS (0.707).

4.4.2.6 RMSE

The RMSE has been recorded to be <0.42 (thereby meaning low error) for all the models during training and validation. The lowest error was recorded, during training, by ANFIS-GA (0.398), with successors: ANFIS-PSO (0.402), ANFIS-DE (0.410), and ANFIS (0.413). The same ranking was also seen, during validation part, for all models. The most successful model ANFIS-GA has recorded lowest error,

RMSE=0.375, following by ANFIS-PSO (0.379), ANFIS-DE (0.387), and ANFIS (0.390).

Apart from above important matrices results, the supplementary parameters i.e. false positive rate, false discovery rate, false negative rate, and Odd-Ratio are also provided in the table 5.

4.4.3 SCAI

Another validation assessment has been performed through SCAI method to check the classification accuracy of produced maps obtained using all the four models. The classification accuracy results are displayed in figure 11. The SCAI calculates the ratio between the class share and the observed flood share for the particular class. And after the analysis of the SCAI values are found low for low susceptible classes (Very low to Moderate classes), it indicates that the classification accuracy is poor for that particular map; also, the high SCAI values for high susceptible classes (High & Very High classes) refers the same low classification accuracy as well. But the results found in this study show that the high SCAI values have been observed for low susceptible classes as well as low SCAI values for high susceptible classes and it proves that the produced maps of all the models are of good to excellent classification accuracy category. The maximum classification accuracy was observed in case of ANFIS-PSO & ANFIS-GA models. The ANFIS based modelled FSPI map shows less accuracy in comparison to the other three models. In order to have better comprehension of the model accuracies, the frequency ratio (FR) based diagram (figure 11A) is also provided along with SCAI diagram (figure 11B).

5. Discussion

5.1 Assessment of variable importance

The assessment of CgFs importance is relevant for planners and decision makers for better utilization of resources and maximum productivity using limited resources allocation (Testa et al., 2016). The derivation of importance of CgFs for spatial modelling using bivariate models computation at the time of analysing their class-wise importance or weightages assignment with the aid of frequency ratio, evidential belief function, Shannon's entropy, Index of entropy, etc. (Arabameri et al., 2019a; Arora et al., 2019). But, application of ML based models requires a pre-analysed weightage or importance assignment to all the CgFs before employment of models for spatial modelling. There are a number of studies available where the relative importance of variables has been computed before spatial modelling using different methods i.e. Analytic Hierarchy Process (AHP) (Pradhan, 2017), Information-Gain method (Costache et al., 2020b), random forest model (Arabameri et al., 2019f), Stepwise Weight Assessment Ratio Analysis (SWARA) (Bui et al., 2018b; Chen et al., 2019), etc. And, there are numerous approaches being continuously used to analyse the relative importance of CgFs for spatial modelling. The performance of different techniques have also been assessed on the same set of CgFs to select the best ones from among list but the importance of CgFs is also affected and determined by the type of topography and data utilized for derivation of those CgFs. Therefore, the performance of models is also compromised due to various factors involved in preparation of CgFs. Hence, the selection of a method for assessing relative importance is not strict or limited to any isolated model. In present work, the random forest model has been used for evaluation of relative importance of each conditioning factor. The validation of the model performance was performed using confusion matrix table (table 4). An amicably acceptable level of accuracy and

precision (~0.70 for both parameters) was recorded by the RF model using the confusion matrix table.

Here, from the list, we can observe that the geomorphology has outperformed all the other CgFs in terms of contributor to the predictability of flood susceptibility. Since, the MGP is predominantly a fluvial environment and the geomorphology dataset carries the most valuable information related to the fluvial form-process relationship represented in form of geomorphological units e.g. active & old floodplain, paleochannel, channel bar, bars, meanders, etc. as well as provide a layout of historical flood events, the model results also verify the predictability importance of geomorphology in its result. The second important factor, distance to stream, in the list as a predictor of flood can be explained as the streams or rivers are prime source of flood in the fluvial environment, especially in plains like the MGP, bringing havoc at recurring interval. At the same time, the curvature and slope are also found as important factors for flood predictability due to almost plain surface topography in the study area. Here, it may be noted that the rainfall, one of the major flood-controlling factors, secured the last position in the analysis. It can be explained as the least factor for flood in MGP due to the location of MGP. The MGP lies in the lower Ganga basin and here three major rivers- Ganga, Ghaghara & Son form a confluence zone, almost in the middle of the study area, means the flood water during monsoon period have been brought by upstream channels including these three major rivers. In fact, when rainfall occurs in upstream channels, the heavy streams bring flooded water in downstream channel stretches of the Ganga river basin. Therefore, in MGP the rainfall couldn’t come up as a chief controlling factor for flood.

5.2 The selection and impact of conditioning factors in FSM

The success of a prediction model is dependent, directly or indirectly, on the selection procedure and type of the conditioning factors. It also determines prediction quality of involved models (Arora et al., 2019; Lee et al., 2017). It can be noted that there is no universal guideline available for selection of conditioning factors as well as their number and class divisions (Khosravi et al., 2018). But the selection of flood controlling CgFs can be affected by the type of topography and climatic conditions. It has been elaborated in the previous study of FSM using bivariate models that the geomorphology has performed better in comparison to geology (lithology) as a contributor to floods in the fluvial floodplain topographic setting such as the MGP (Arora et al., 2019); therefore, in present study the more refined version of geomorphology dataset has been selected. Including geomorphology, total twelve CgFs have been selected in this study keeping in mind the existing fluvial setup and hydro-climatological conditions of the MGP. The preferability of geomorphology over geology is also justified by the variable importance analysis using RF model. Wherein, the geomorphology as a contributing factor is listed on top with the maximum weightage as opposed to other controlling factors for flood. The other impactful CgFs have been noted, after factor importance analysis results which are stream density, distance to stream, TWI, Slope, and curvature.

5.3 The model performance evaluation and comparison

All the heuristic models, ANFIS & their ensembles, performed very well and the assessment of their performance were also verified by the AUCROC method including other dependent metrices. The AUC for all four models ranges between 0.768 and 0.924 during training and validation parts. The most promising model, ANFIS-GA_{SR} (AUC=0.922) & ANFIS-GA_{PR} (AUC=0.924), has secured the top position in comparison to remaining models. There has been no potential study

857 conducted in MGP or in any other similar topographic settings in India to date for
858 FSM by using the ANFIS & ensembles models, therefore, in comparison with other
859 similar kind of work it has been observed that the performance of results are found
860 better to the study conducted by Hong et al. (2018) using ANFIS-DE (AUC_{SR} =
861 0.8523, AUC_{PR}= 0.8686) & ANFIS-GA (AUC_{SR} = 0.8488, AUC_{PR}= 0.8743) models in
862 Hengfeng County, China (Hong et al., 2018a). The varied difference in both results
863 using same models may occur due to different topographic configuration and
864 selection of CgFs. In comparison to another study conducted by M. Ahmadlou et al.
865 (2019) for Iran using ANSIF & ensembles using biogeography-based optimization
866 (BBO) and BAT algorithm (BA) (ANFIS-BBO & ANFIS-BAT) (Ahmadlou et al., 2019),
867 the performance of used models in present study have found much better during
868 training & validation. In earlier work, the maximum AUC was recorded for both
869 ANFIS-BBO & ANFIS-BAT (AUC=0.77) during training and AUC=0.70 was recorded
870 during testing for both models. Whereas, in present work, even the lowest
871 performing ANFIS model has performed better than both models.

872 In the study conducted by Hong et al. (2018), the altitude range recorded at some
873 places are ~1340 meter which indicates that the topography of the study area was
874 not plain topography compared to the MGP topographic setting where the maximum
875 altitude is recorded ~100 meter only and the elevation range is ~83m. Another
876 important point observed between both studies is that the present study used the
877 geomorphology as a flood controlling factor keeping in mind fluvial topographic
878 setting in the present MGP area whereas, Hong et al. did not.

879 Apart from these major geo-environmental factors' selection, other reasons for
880 variations in model performance maybe counted in the quality of preparation of flood
881 inventory, the number of flood and non-flood point generation and utilization of

training & testing points as samples, data processing, and preparation of CgFs using satellite images; where the calibration, resolution (spatial & temporal), & size of input data (satellite images or in-situ data).

Having acquired all the performance facets of models employed in this study, it will be helpful to the hazard managers, both national and local level managers, to have an idea about which areas are most susceptible to flooding and which ones are least. Also, the sequence of contributing factors used for flood occurrence potential prediction or flood susceptibility prediction, the authorities will be able to priorities their efforts to apply nature based solutions (NBS) like creating natural embankments, or making tree barriers, etc. or other NBS as per the suitability of the measures' to help curb the detrimental effects of the factors. Gómez Martín et al., (2020) have suggested two classifications of NBS: 1) horizontal NBS framework; and 2) vertical NBS framework. Horizontal NBS framework advocate for levels of human intervention in the solution measures and based on this, three types of horizontal NSB are suggested: a) NBS type 1; b) NBS type 2; and c) NBS type 3; NBS type 1 involves low human intervention and type 3 involves higher levels of modifications in the ecosystem. Green, blue, or grey infrastructural measures of NBS are suggested for city based flood inundation related management practices (Commission, 2015; Eggermont et al., 2015, 2015; Faivre et al., 2017). Geomorphology being the most important factor contributing to the flood susceptibility prediction in this low altitudinal subtropical monsoonal topoclimatic regions, the NBS of simplest type will be to identify geomorphic units which are flooded regularly and which are most inhabited or occupied for economic activities, NBS types 1, 2, or 3, should be applied for sustainable development of the area.

6. Conclusions

907 The Central Gangetic floodplains being one of the worst flood affected regions in the
908 world still lag proper natural hazard actionable policies crafted to tackle the losses
909 due to this menace. In order to execute the effectively actionable decision-making
910 process in this critically flood affected region, aim should be reducing losses related
911 to hydraulic projects for sustainable development, developing sites for industrial hub
912 demarcation and settlement areas, the updated, accurate, verifiable flood prone
913 areas, their susceptibility, etc. are of prime significance. The present work has been
914 carried out with an impetus to fulfil the data lag in this frequently flooded part of the
915 MGP region located in the Ganga River Basin, India, during monsoon period (June
916 to October), improvements in the model performances warrants an improved quality
917 of model input parameters. In our present work, the inclusion of upgraded
918 geomorphology dataset as a higher quality conditioning factor has helped in
919 improving the accuracy of the model ensembles. The RF model analysis has
920 revealed the highest relative importance of the geomorphology among all CgFs.
921 Comparison of results with the previous study conducting the FSM in the same part
922 of the MGP applying FR & Shannon's entropy (SE)(Arora et al., 2019) signifies the
923 fact that there is achieved an improvement is achieved in the performance of the
924 advanced and novel ensemble models, not previously used by any workers for flood
925 susceptibility zonation in any part of India. The present work used the ANFIS & novel
926 ensembles and recorded better accuracy than models used in earlier study in the
927 same topoclimatic environmental setting. Among all the four used models in present
928 work, the ANFIS-GA has come up to be the best performant after assessing all
929 models' training & testing performances by independent (AUROC) & multiple
930 dependent metrices methods i.e. accuracy, prediction, F-Score, Cohen's Kappa, etc.
931 The results and comparison also show that the selection & optimization of CgFs may

also improve the accuracy of models for prediction. It is also noted that the ensembles have performed better than the isolated individual ANFIS model. The efficacy and accuracy of all ensembles have also been noted better during training and testing stages. Also, the coverages of high susceptible lands for flood resonated better with flood samples for the ensemble-based produced maps than ANFIS based map.

Like other studies aiming to achieve the model universality, this study too has its own constraints and limitations related to DEM data quality, model configuration related limitations, algorithms' assumptions, etc. but more and better advancement on these frontiers of flood susceptibility zonation modelling is still under progress and more such studies with better field related data will be needed to help improve the precision and accuracy of such modelling exercises aimed at sustainable development of such flood affected areas.

Studies like this can be viewed as beneficial in two time frames: 1) present day; and 2) future. The future flood menace presenting challenges to the natural hazard management authorities in the present timeframe will help in gaining information related to what factors are more important contributors in flood occurrence potential prediction and thus, help to focus their attention to take nature based solution measures to control the flood waters reaching such places. And secondly, the flood susceptibility zonation maps will lead to overall fund allocation for different zones depending upon the potential damages probable in those zones. As far as future flood scenarios are concerned, since we are heading towards an era of 'space based monitoring, analysis, assessment and evaluation" of all natural (both biotic and abiotic) and manmade phenomena, the intensive testing (Abdelghafar et al., 2020; Alsdorf et al., 2003; DeVries et al., 2020; Green et al., 2020; Hassanien et al., 2020;

Kummerow et al., 2020; Malinowska et al., 2020; Salisbury et al., 2013; Spyropoulos et al., 2020; Sterckx et al., 2020; Tang et al., 2010; Thies and Bendix, 2011; Tonetti et al., 2020), and different machine learning algorithms are being developed and already existing ones are being tested and validated considering all possible scenarios including different types of topoclimatic settings. In flood hazard management science, the modelling community is engaged in developing, testing and validating models for different environmental settings. But, till date, this dimension of model testing as per variability of topoclimatic and hydrometeorological differences has recently been mulled and promulgated by Arora et al. 2019. Arora and his team have attempted developing, testing and validating all types of susceptibility models, starting from simplest 'frequency ratio (FR)' and 'Shannon Entropy (SE)" models to more complex ones like for low altitudinal range floodplain environment. There is a need to test all existing types of models e.g. other machine learning standalone and ensembles of MLP (multiplayer perceptron), LR (logistic regression), CART (classification and regression tree), SVM (support vector machine), etc. with other categories of models like FR, EBF (evidential belief function), etc. After critical comparison of all types of models' performances in different topoclimatic and hydrometeorological settings, the best performing models may be suggested to be set in automated future satellite missions that will able to provide Near Real Time Flood Monitoring and Susceptibility Prediction viz. SWOT satellite mission (Morrow et al., 2019) that provides topographic and surface water information at very fine temporal and spatial resolutions for the world oceans.

References

Abdelghafar, S., Darwish, A., Hassanien, A.E., 2020. Intelligent Health Monitoring Systems for Space Missions Based on Data Mining Techniques, in: Hassanien

A., Darwish A., E.-A.H. (eds) (Ed.), Machine Learning and Data Mining in Aerospace Technology. Studies in Computational Intelligence. Springer, Cham, pp. 65–78. doi:10.1007/978-3-030-20212-5_4

Achour, Y., Pourghasemi, H.R., 2020. How do machine learning techniques help in increasing accuracy of landslide susceptibility maps? Geosci. Front. 11, 871–883. doi:10.1016/j.gsf.2019.10.001

Ahmadlou, M., Karimi, M., Alizadeh, S., Shirzadi, A., Parvinnejhad, D., Shahabi, H., Panahi, M., 2019. Flood susceptibility assessment using integration of adaptive network-based fuzzy inference system (ANFIS) and biogeography-based optimization (BBO) and BAT algorithms (BA). Geocarto Int. 34, 1252–1272. doi:10.1080/10106049.2018.1474276

Alabyan, A.M., Chalov, R.S., 1998. Types of river channel patterns and their natural controls. Earth Surf. Process. Landforms 23, 467–474. doi:10.1002/(SICI)1096-9837(199805)23:5<467::AID-ESP861>3.0.CO;2-T

Alin, A., 2010. Multicollinearity. Wiley Interdiscip. Rev. Comput. Stat. 2, 370–374. doi:10.1002/wics.84

Alsdorf, D., Lettenmaier, D., Vörösmarty, C., 2003. The need for global, satellite-based observations of terrestrial surface waters. Eos, Trans. Am. Geophys. Union 84, 269–276. doi:10.1029/2003EO290001

Arabameri, A., Cerda, A., Tiefenbacher, J.P., 2019a. Spatial Pattern Analysis and Prediction of Gully Erosion Using Novel Hybrid Model of Entropy-Weight of Evidence. Water 11, 1129. doi:10.3390/w11061129

Arabameri, A., Chen, W., Lombardo, L., Blaschke, T., Tien Bui, D., 2020a. Hybrid

1005 Computational Intelligence Models for Improvement Gully Erosion Assessment.
1006 Remote Sens. 12, 140. doi:10.3390/rs12010140

1007 Arabameri, A., Pradhan, B., Bui, D.T., 2020b. Spatial modelling of gully erosion in
1008 the Ardib River Watershed using three statistical-based techniques. CATENA
1009 190, 104545. doi:10.1016/j.catena.2020.104545

1010 Arabameri, A., Pradhan, B., Lombardo, L., 2019b. Comparative assessment using
1011 boosted regression trees, binary logistic regression, frequency ratio and
1012 numerical risk factor for gully erosion susceptibility modelling. CATENA 183,
1013 104223. doi:10.1016/j.catena.2019.104223

1014 Arabameri, A., Pradhan, B., Rezaei, K., 2019c. Spatial prediction of gully erosion
1015 using ALOS PALSAR data and ensemble bivariate and data mining models.
1016 Geosci. J. 23, 669–686. doi:10.1007/s12303-018-0067-3

1017 Arabameri, A., Pradhan, B., Rezaei, K., 2019d. Gully erosion zonation mapping
1018 using integrated geographically weighted regression with certainty factor and
1019 random forest models in GIS. J. Environ. Manage. 232, 928–942.
1020 doi:10.1016/j.jenvman.2018.11.110

1021 Arabameri, A., Rezaei, K., Cerdà, A., Conoscenti, C., Kalantari, Z., 2019e. A
1022 comparison of statistical methods and multi-criteria decision making to map
1023 flood hazard susceptibility in Northern Iran. Sci. Total Environ. 660, 443–458.
1024 doi:10.1016/j.scitotenv.2019.01.021

1025 Arabameri, A., Yamani, M., Pradhan, B., Melesse, A., Shirani, K., Tien Bui, D.,
1026 2019f. Novel ensembles of COPRAS Multi-criteria decision-making with logistic
1027 regression, boosted regression tree, and random forest for spatial prediction of

1028 gully erosion susceptibility. Sci. Total Environ. 688.
1029 doi:10.1016/j.scitotenv.2019.06.205

1030 Arora, A., Pandey, M., Siddiqui, M.A., Hong, H., Mishra, V.N., 2019. Spatial flood
1031 susceptibility prediction in Middle Ganga Plain: comparison of frequency ratio
1032 and Shannon's entropy models. Geocarto Int. 1–32.
1033 doi:10.1080/10106049.2019.1687594

1034 Barredo, J.I., 2009. Normalised flood losses in Europe: 1970-2006. Nat. Hazards
1035 Earth Syst. Sci. 9.

1036 Bartier, P.M., Keller, C.P., 1996. Multivariate interpolation to incorporate thematic
1037 surface data using inverse distance weighting (IDW). Comput. Geosci. 22, 795–
1038 799. doi:10.1016/0098-3004(96)00021-0

1039 Bhowmik, N.G., Stall, J.B., 1979. Hydraulic geometry and carrying capacity of
1040 floodplains.

1041 Booker, L.B., Goldberg, D.E., Holland, J.H., 1989. Classifier systems and genetic
1042 algorithms. Artif. Intell. 40, 235–282. doi:https://doi.org/10.1016/0004-
1043 3702(89)90050-7

1044 Boulton, S.J., Stokes, M., 2018. Which DEM is best for analyzing fluvial landscape
1045 development in mountainous terrains? Geomorphology 310, 168–187.
1046 doi:10.1016/j.geomorph.2018.03.002

1047 Bui, D.T., Khosravi, K., Li, S., Shahabi, H., Panahi, M., Singh, V.P., Chapi, K.,
1048 Shirzadi, A., Panahi, S., Chen, W., Bin Ahmad, B., 2018a. New hybrids of
1049 ANFIS with several optimization algorithms for flood susceptibility modeling.
1050 Water (Switzerland). doi:10.3390/w10091210

1051 Bui, D.T., Panahi, M., Shahabi, H., Singh, V.P., Shirzadi, A., Chapi, K., Khosravi, K.,
1052 Chen, W., Panahi, S., Li, S., Ahmad, B. Bin, 2018b. Novel Hybrid Evolutionary
1053 Algorithms for Spatial Prediction of Floods. Sci. Rep. 8, 15364.
1054 doi:10.1038/s41598-018-33755-7

1055 Bui, D.T., Tsangaratos, P., Ngo, P.-T.T., Pham, T.D., Pham, B.T., 2019. Flash flood
1056 susceptibility modeling using an optimized fuzzy rule based feature selection
1057 technique and tree based ensemble methods. Sci. Total Environ. 668, 1038–
1058 1054. doi:10.1016/j.scitotenv.2019.02.422

1059 Cai, Y.P., Huang, G.H., Tan, Q., Chen, B., 2011. Identification of optimal strategies
1060 for improving eco-resilience to floods in ecologically vulnerable regions of a
1061 wetland. Ecol. Modell. 222, 360–369. doi:10.1016/j.ecolmodel.2009.12.012

1062 Catalão, J.P.S., Pousinho, H.M.I., Mendes, V.M.F., 2011. Hybrid wavelet-PSO-
1063 ANFIS approach for short-term electricity prices forecasting. IEEE Trans. Power
1064 Syst. 26, 137–144. doi:10.1109/TPWRS.2010.2049385

1065 Chai, T., Draxler, R.R., 2014. Root mean square error (RMSE) or mean absolute
1066 error (MAE)? -Arguments against avoiding RMSE in the literature. Geosci.
1067 Model Dev. 7, 1247–1250. doi:10.5194/gmd-7-1247-2014

1068 Chapi, K., Singh, V.P., Shirzadi, A., Shahabi, H., Bui, D.T., Pham, B.T., Khosravi, K.,
1069 2017a. CO.

1070 Chapi, K., Singh, V.P., Shirzadi, A., Shahabi, H., Bui, D.T., Pham, B.T., Khosravi, K.,
1071 2017b. A novel hybrid artificial intelligence approach for flood susceptibility
1072 assessment. Environ. Model. Softw. 95, 229–245.
1073 doi:10.1016/j.envsoft.2017.06.012

1074 Chen, H.T., Chen, X.N., Qiu, L., Wang, W.C., 2020. Multi-objective ecological
1075 operation of reservoir in Luanhe river based on improved particle swarm
1076 optimization. Nat. Environ. Pollut. Technol. 19, 113–121.

1077 Chen, W., Panahi, M., Tsangaratos, P., Shahabi, H., Ilia, I., Panahi, S., Li, S.,
1078 Jaafari, A., Ahmad, B. Bin, 2019. Applying population-based evolutionary
1079 algorithms and a neuro-fuzzy system for modeling landslide susceptibility.
1080 CATENA 172, 212–231. doi:10.1016/j.catena.2018.08.025

1081 Chen, W., Shahabi, H., Shirzadi, A., Hong, H., Akgun, A., Tian, Y., Liu, J., Zhu, A.X.,
1082 Li, S., 2018. Novel hybrid artificial intelligence approach of bivariate statistical-
1083 methods-based kernel logistic regression classifier for landslide susceptibility
1084 modeling. Bull. Eng. Geol. Environ. doi:10.1007/s10064-018-1401-8

1085 Choubin, B., Moradi, E., Golshan, M., Adamowski, J., Sajedi-Hosseini, F., Mosavi,
1086 A., 2019a. An ensemble prediction of flood susceptibility using multivariate
1087 discriminant analysis, classification and regression trees, and support vector
1088 machines. Sci. Total Environ. 651, 2087–2096.
1089 doi:10.1016/j.scitotenv.2018.10.064

1090 Choubin, B., Rahmati, O., Soleimani, F., Alilou, H., Moradi, E., Alamdari, N., 2019b.
1091 Regional groundwater potential analysis using classification and regression
1092 trees, in: Spatial Modeling in GIS and R for Earth and Environmental Sciences.
1093 Elsevier, pp. 485–498.

1094 Cohen, J., 1960. A Coefficient of Agreement for Nominal Scales. Educ. Psychol.
1095 Meas. 20, 37–46. doi:10.1177/001316446002000104

1096 Commission, E., 2015. Towards an EU Research and Innovation Policy Agenda for

1097 Nature-Based Solutions & Re-Naturing Cities. Final Report of the Horizon 2020
1098 Expert Group on ‘Nature-Based Solutions and Re-Naturing Cities. Publications
1099 Office of the European Union Luxembourg.

1100 Costache, R., Hong, H., Pham, Q.B., 2020a. Comparative assessment of the flash-
1101 flood potential within small mountain catchments using bivariate statistics and
1102 their novel hybrid integration with machine learning models. Sci. Total Environ.
1103 711, 134514. doi:10.1016/j.scitotenv.2019.134514

1104 Costache, R., Pham, Q.B., Avand, M., Thuy Linh, N.T., Vojtek, M., Vojteková, J.,
1105 Lee, S., Khoi, D.N., Thao Nhi, P.T., Dung, T.D., 2020b. Novel hybrid models
1106 between bivariate statistics, artificial neural networks and boosting algorithms for
1107 flood susceptibility assessment. J. Environ. Manage. 265.
1108 doi:10.1016/j.jenvman.2020.110485

1109 Costache, R., Pham, Q.B., Sharifi, E., Linh, N.T.T., Abba, S.I., Vojtek, M., Vojteková,
1110 J., Nhi, P.T.T., Khoi, D.N., 2020c. Flash-flood susceptibility assessment using
1111 multi-criteria decision making and machine learning supported by remote
1112 sensing and GIS techniques. Remote Sens. doi:10.3390/RS12010106

1113 Costache, R., Tien Bui, D., 2019. Spatial prediction of flood potential using new
1114 ensembles of bivariate statistics and artificial intelligence: A case study at the
1115 Putna river catchment of Romania. Sci. Total Environ. 691, 1098–1118.
1116 doi:10.1016/j.scitotenv.2019.07.197

1117 CRED, 2016. EM-DAT | The international disasters database website [WWW
1118 Document]. Cent. Res. Epidemiol. Disasters (CRED), Univ. Cathol. Louvain.
1119 URL https://www.emdat.be/ (accessed 6.7.19).

1120 DeVries, B., Huang, C., Armston, J., Huang, W., Jones, J.W., Lang, M.W., 2020.
1121 Rapid and robust monitoring of flood events using Sentinel-1 and Landsat data
1122 on the Google Earth Engine. Remote Sens. Environ. 240, 111664.
1123 doi:10.1016/j.rse.2020.111664

1124 Dimri, A.P., Kumar, D., Chopra, S., Choudhary, A., 2019. Indus River Basin: Future
1125 climate and water budget. Int. J. Climatol. 39, 395–406. doi:10.1002/joc.5816

1126 Đurić, U., Marjanović, M., Radić, Z., Abolmasov, B., 2019. Machine learning based
1127 landslide assessment of the Belgrade metropolitan area: Pixel resolution effects
1128 and a cross-scaling concept. Eng. Geol. doi:10.1016/j.enggeo.2019.05.007

1129 Eggermont, H., Balian, E., Azevedo, J.M.N., Beumer, V., Brodin, T., Claudet, J.,
1130 Fady, B., Grube, M., Keune, H., Lamarque, P., Reuter, K., Smith, M., van Ham,
1131 C., Weisser, W.W., Le Roux, X., 2015. Nature-based Solutions: New Influence
1132 for Environmental Management and Research in Europe. GAIA - Ecol. Perspect.
1133 Sci. Soc. 24, 243–248. doi:10.14512/gaia.24.4.9

1134 Faivre, N., Fritz, M., Freitas, T., de Boissezon, B., Vandewoestijne, S., 2017. Nature-
1135 Based Solutions in the EU: Innovating with nature to address social, economic
1136 and environmental challenges. Environ. Res. 159, 509–518.
1137 doi:10.1016/j.envres.2017.08.032

1138 Field, J., 2001. Channel avulsion on alluvial fans in southern Arizona.
1139 Geomorphology 37, 93–104. doi:10.1016/S0169-555X(00)00064-7

1140 Fressard, M., Thiery, Y., Maquaire, O., 2014. Which data for quantitative landslide
1141 susceptibility mapping at operational scale? Case study of the Pays d'Auge
1142 plateau hillslopes (Normandy, France). Nat. Hazards Earth Syst. Sci. 14, 569–

588. doi:10.5194/nhess-14-569-2014

Gómez Martín, E., Máñez Costa, M., Schwerdtner Máñez, K., 2020. An operationalized classification of Nature Based Solutions for water-related hazards: From theory to practice. Ecol. Econ. 167, 106460. doi:10.1016/j.ecolecon.2019.106460

Green, J., Draper, D., Grant, H., Rall, J., 2020. Scientific Discovery and Geomagnetic Monitoring in Earth Orbit Using Small Satellite Systems, in: Handbook of Small Satellites. Springer International Publishing, Cham, pp. 1–19. doi:10.1007/978-3-030-20707-6_35-1

Hair, J.F., Black, W.C., Babin, B.J., Anderson, R.E., 2013. Multivariate Data Analysis, Pearson New International Edition, 7th Edition, 7th ed. Pearson Higher Ed.

Hallegatte, S., Green, C., Nicholls, R.J., Corfee-Morlot, J., 2013. Future flood losses in major coastal cities. Nat. Clim. Chang. 3, 802–806. doi:10.1038/nclimate1979

Hanson, S., Nicholls, R., Ranger, N., Hallegatte, S., Corfee-Morlot, J., Herweijer, C., Chateau, J., 2011. A global ranking of port cities with high exposure to climate extremes. Clim. Change 104, 89–111. doi:10.1007/s10584-010-9977-4

Häring, T., Dietz, E., Osenstetter, S., Koschitzki, T., Schröder, B., 2012. Spatial disaggregation of complex soil map units: A decision-tree based approach in Bavarian forest soils. Geoderma 185–186, 37–47. doi:10.1016/j.geoderma.2012.04.001

Harris, R.R., 1987. Occurrence of Vegetation on Geomorphic Surfaces in the Active Floodplain of a California Alluvial Stream. Am. Midl. Nat. 118, 393.

doi:10.2307/2425796

Hassanien, A.E., Darwish, A., Abdelghafar, S., 2020. Machine learning in telemetry data mining of space mission: basics, challenging and future directions. Artif. Intell. Rev. 53, 3201–3230. doi:10.1007/s10462-019-09760-1

Hayakawa, Y.S., Oguchi, T., Lin, Z., 2008. Comparison of new and existing global digital elevation models: ASTER G-DEM and SRTM-3. Geophys. Res. Lett. 35, L17404. doi:10.1029/2008GL035036

Hoehler, F.K., 2000. Bias and prevalence effects on kappa viewed in terms of sensitivity and specificity. J. Clin. Epidemiol. 53, 499–503. doi:https://doi.org/10.1016/S0895-4356(99)00174-2

Hong, H., Panahi, M., Shirzadi, A., Ma, T., Liu, J., Zhu, A.-X., Chen, W., Kougias, I., Kazakis, N., 2018a. Flood susceptibility assessment in Hengfeng area coupling adaptive neuro-fuzzy inference system with genetic algorithm and differential evolution. Sci. Total Environ. 621, 1124–1141. doi:10.1016/j.scitotenv.2017.10.114

Hong, H., Panahi, M., Shirzadi, A., Ma, T., Liu, J., Zhu, A.X., Chen, W., Kougias, I., Kazakis, N., 2018b. Flood susceptibility assessment in Hengfeng area coupling adaptive neuro-fuzzy inference system with genetic algorithm and differential evolution. Sci. Total Environ. 621, 1124–1141. doi:10.1016/j.scitotenv.2017.10.114

Hu, J.W., 2016. Advanced Materials and Structural Engineering: Proceedings of the International Conference on Advanced Materials and Engineering Structural Technology (ICAMEST 2015), April 25-26, 2015, Qingdao, China. CRC Press.

1189 Hudson, P.F., 2017. Fluvial Depositional Processes and Landforms, in: International
1190 Encyclopedia of Geography: People, the Earth, Environment and Technology.
1191 John Wiley & Sons, Ltd, Oxford, UK, pp. 1–9.
1192 doi:10.1002/9781118786352.wbieg0872

1193 Jaafari, A., Panahi, M., Pham, B.T., Shahabi, H., Bui, D.T., Rezaie, F., Lee, S., 2019.
1194 Meta optimization of an adaptive neuro-fuzzy inference system with grey wolf
1195 optimizer and biogeography-based optimization algorithms for spatial prediction
1196 of landslide susceptibility. CATENA 175, 430–445.
1197 doi:10.1016/j.catena.2018.12.033

1198 Jacobson, R., Faust, T., 2014. HYDROLOGIC CONNECTIVITY OF FLOODPLAINS,
1199 NORTHERN MISSOURI-IMPLICATIONS FOR MANAGEMENT AND
1200 RESTORATION OF FLOODPLAIN FOREST COMMUNITIES IN DISTURBED
1201 LANDSCAPES. River Res. Appl. 30, 269–286. doi:10.1002/rra.2636

1202 Jang, J.R., 1993. ANFIS : Adap tive-Ne twork-Based Fuzzy Inference System 23.

1203 Junk, W.J., Bayley, P.B., Sparks, R.E., 1989. The flood pulse concept in river-
1204 floodplain systems. Can. Spec. Publ. Fish. Aquat. Sci.
1205 doi:10.1371/journal.pone.0028909

1206 Keesstra, S., Mol, G., de Leeuw, J., Okx, J., Molenaar, C., de Cleen, M., Visser, S.,
1207 2018. Soil-Related Sustainable Development Goals: Four Concepts to Make
1208 Land Degradation Neutrality and Restoration Work. Land 7, 133.
1209 doi:10.3390/land7040133

1210 Keesstra, S.D., Bouma, J., Wallinga, J., Tittonell, P., Smith, P., Cerdà, A.,
1211 Montanarella, L., Quinton, J.N., Pachepsky, Y., van der Putten, W.H., Bardgett,

1212 R.D., Moolenaar, S., Mol, G., Jansen, B., Fresco, L.O., 2016. The significance of
1213 soils and soil science towards realization of the United Nations Sustainable
1214 Development Goals. SOIL 2, 111–128. doi:10.5194/soil-2-111-2016

1215 Kennedy, J., Eberhart, R., 1995. Particle swarm optimization, in: Proceedings of
1216 ICNN'95 - International Conference on Neural Networks. pp. 1942–1948 vol.4.
1217 doi:10.1109/ICNN.1995.488968

1218 Khosravi, K., Nohani, E., Maroufinia, E., Pourghasemi, H.R., 2016a. A GIS-based
1219 flood susceptibility assessment and its mapping in Iran: a comparison between
1220 frequency ratio and weights-of-evidence bivariate statistical models with multi-
1221 criteria decision-making technique. Nat. Hazards 83, 947–987.
1222 doi:10.1007/s11069-016-2357-2

1223 Khosravi, K., Panahi, M., Tien Bui, D., 2018. Spatial prediction of groundwater spring
1224 potential mapping based on an adaptive neuro-fuzzy inference system and
1225 metaheuristic optimization. Hydrol. Earth Syst. Sci. 22, 4771–4792.
1226 doi:10.5194/hess-22-4771-2018

1227 Khosravi, K., Pourghasemi, H.R., Chapi, K., Bahri, M., 2016b. Flash flood
1228 susceptibility analysis and its mapping using different bivariate models in Iran: a
1229 comparison between Shannon's entropy, statistical index, and weighting factor
1230 models. Environ. Monit. Assess. 188. doi:10.1007/s10661-016-5665-9

1231 Khosravi, K., Shahabi, H., Pham, B.T., Adamowski, J., Shirzadi, A., Pradhan, B.,
1232 Dou, J., Ly, H.B., Gróf, G., Ho, H.L., Hong, H., Chapi, K., Prakash, I., 2019. A
1233 comparative assessment of flood susceptibility modeling using Multi-Criteria
1234 Decision-Making Analysis and Machine Learning Methods. J. Hydrol. 573, 311–

323. doi:10.1016/j.jhydrol.2019.03.073

Kummerow, C.D., Tanelli, S., Takahashi, N., Furukawa, K., Klein, M., Levizzani, V., 2020. Plans for Future Missions, in: Levizzani V., Kidd C., Kirschbaum D., Kummerow C., Nakamura K., T.F. (eds) (Ed.), Satellite Precipitation Measurement. Advances in Global Change Research. Springer, Cham., pp. 99–119. doi:10.1007/978-3-030-24568-9_6

Lee, Sunmin, Kim, J.C., Jung, H.S., Lee, M.J., Lee, Saro, 2017. Spatial prediction of flood susceptibility using random-forest and boosted-tree models in Seoul metropolitan city, Korea. Geomatics, Nat. Hazards Risk 8, 1185–1203. doi:10.1080/19475705.2017.1308971

Lei, Y., He, Z., Zi, Y., Hu, Q., 2007. Fault diagnosis of rotating machinery based on multiple ANFIS combination with GAs. Mech. Syst. Signal Process. 21, 2280–2294. doi:10.1016/j.ymssp.2006.11.003

Li, K., Su, H., 2010. Forecasting building energy consumption with hybrid genetic algorithm-hierarchical adaptive network-based fuzzy inference system. Energy Build. 42, 2070–2076. doi:10.1016/j.enbuild.2010.06.016

Li, W., MacBean, N., Ciais, P., Defourny, P., Lamarche, C., Bontemps, S., Houghton, R.A., Peng, S., 2018. Gross and net land cover changes in the main plant functional types derived from the annual ESA CCI land cover maps (1992–2015). Earth Syst. Sci. Data 10, 219–234. doi:10.5194/essd-10-219-2018

Liu, H., Li, G., 2005. Testing Statistical Significance of the Area under a Receiving Operating Characteristics Curve for Repeated Measures Design with Bootstrapping. J. Data Sci. 3, 257–278.

1258 Lunt, I.A., Bridge, J.S., 2004. Evolution and deposits of a gravelly braid bar,
1259 Sagavanirktok River, Alaska. Sedimentology 51, 415–432. doi:10.1111/j.1365-
1260 3091.2004.00628.x

1261 Malinowska, A.A., Witkowski, W.T., Guzy, A., Hejmanowski, R., 2020. Satellite-
1262 Based Monitoring and Modeling of Ground Movements Caused by Water
1263 Rebound. Remote Sens. 12, 1786. doi:10.3390/rs12111786

1264 Marzban, C., 2004. The ROC Curve and the Area under It as Performance
1265 Measures. Weather Forecast. 19, 1106–1114. doi:10.1175/825.1

1266 McCall, J., 2005. Genetic algorithms for modelling and optimisation. J. Comput. Appl.
1267 Math. 184, 205–222. doi:https://doi.org/10.1016/j.cam.2004.07.034

1268 Mehrabi, M., Pradhan, B., Moayedi, H., Alamri, A., 2020. Optimizing an adaptive
1269 neuro-fuzzy inference system for spatial prediction of landslide susceptibility
1270 using four state-of-the-art metaheuristic techniques. Sensors (Switzerland) 20.
1271 doi:10.3390/s20061723

1272 Menard, S., 2002. Applied logistic regression analysis. Sage.

1273 Merz, B., Thieken, A.H., Gocht, M., 2007. Flood risk mapping at the local scale:
1274 Concepts and challenges. Adv. Nat. Technol. Hazards Res. 25, 231–251.
1275 doi:10.1007/978-1-4020-4200-3_13

1276 Moayedi, H., Khari, M., Bahiraei, M., Foong, L.K., Bui, D.T., 2020. Spatial
1277 assessment of landslide risk using two novel integrations of neuro-fuzzy system
1278 and metaheuristic approaches; Ardabil Province, Iran. Geomatics, Nat. Hazards
1279 Risk 11, 230–258. doi:10.1080/19475705.2020.1713234

1280 Morrow, R., Fu, L.-L., Ardhuin, F., Benkiran, M., Chapron, B., Cosme, E., D'Ovidio,
1281 F., Farrar, J.T., Gille, S.T., Lapeyre, G., Le Traon, P.-Y., Pascual, A., Ponte, A.,
1282 Qiu, B., Rascle, N., Ubelmann, C., Wang, J., Zaron, E.D., 2019. Global
1283 Observations of Fine-Scale Ocean Surface Topography With the Surface Water
1284 and Ocean Topography (SWOT) Mission. Front. Mar. Sci. 6.
1285 doi:10.3389/fmars.2019.00232

1286 Naderloo, L., Alimardani, R., Omid, M., Sarmadian, F., Javadikia, P., Torabi, M.Y.,
1287 Alimardani, F., 2012. Application of ANFIS to predict crop yield based on
1288 different energy inputs. Meas. J. Int. Meas. Confed. 45, 1406–1413.
1289 doi:10.1016/j.measurement.2012.03.025

1290 Najafi, B., Faizollahzadeh Ardabili, S., 2018. Application of ANFIS, ANN, and logistic
1291 methods in estimating biogas production from spent mushroom compost (SMC).
1292 Resour. Conserv. Recycl. 133, 169–178. doi:10.1016/j.resconrec.2018.02.025

1293 Oh, H.J., Kadavi, P.R., Lee, C.W., Lee, S., 2018. Evaluation of landslide
1294 susceptibility mapping by evidential belief function, logistic regression and
1295 support vector machine models. Geomatics, Nat. Hazards Risk 9, 1053–1070.
1296 doi:10.1080/19475705.2018.1481147

1297 Onuşluel Gül, G., 2013. Estimating flood exposure potentials in Turkish catchments
1298 through index-based flood mapping. Nat. Hazards. doi:10.1007/s11069-013-
1299 0717-8

1300 Pepe, M.S., Janes, H., Longton, G.M., Leisenring, W., Newcomb, P., 2005.
1301 Limitations of the Odds Ratio in Gauging the Performance of a Diagnostic or
1302 Prognostic Marker.

Pham, Shirzadi, Shahabi, Omidvar, Singh, Sahana, Asl, Ahmad, Quoc, Lee, 2019. Landslide Susceptibility Assessment by Novel Hybrid Machine Learning Algorithms. Sustainability 11, 4386. doi:10.3390/su11164386

Pradhan, B., 2017. Laser scanning applications in landslide assessment. Laser Scanning Appl. Landslide Assess. 1–359. doi:10.1007/978-3-319-55342-9

Price, K., Storn, R.M., Lampinen, J.A., 2006. Differential Evolution: A Practical Approach to Global Optimization, Natural Computing Series. Springer Berlin Heidelberg.

Rahmati, O., Kornejady, A., Samadi, M., Deo, R.C., Conoscenti, C., Lombardo, L., Dayal, K., Taghizadeh-Mehrjardi, R., Pourghasemi, H.R., Kumar, S., Bui, D.T., 2019. PMT: New analytical framework for automated evaluation of geo-environmental modelling approaches. Sci. Total Environ. 664, 296–311. doi:10.1016/j.scitotenv.2019.02.017

Rahmati, O., Pourghasemi, H.R., Zeinivand, H., 2016. Flood susceptibility mapping using frequency ratio and weights-of-evidence models in the Golastan Province, Iran. Geocarto Int. 31, 42–70. doi:10.1080/10106049.2015.1041559

Razavi Termeh, S.V., Kornejady, A., Pourghasemi, H.R., Keesstra, S., 2018. Flood susceptibility mapping using novel ensembles of adaptive neuro fuzzy inference system and metaheuristic algorithms. Sci. Total Environ. 615, 438–451. doi:10.1016/j.scitotenv.2017.09.262

Republic, C., n.d. Forecasting energy consumption using ensemble ARIMA-ANFIS hybrid algorithm Sasan Barak* 1 , S.Saeedeh Sadegh 2 1.

Sachdeva, S., Bhatia, T., Verma, A.K., 2017. Flood susceptibility mapping using

GIS-based support vector machine and particle swarm optimization: A case study in Uttarakhand (India), in: 2017 8th International Conference on Computing, Communication and Networking Technologies (ICCCNT). IEEE, pp. 1–7. doi:10.1109/ICCCNT.2017.8204182

Salisbury, D.J., Anguelova, M.D., Brooks, I.M., 2013. On the variability of whitecap fraction using satellite-based observations. J. Geophys. Res. Ocean. 118, 6201–6222. doi:10.1002/2013JC008797

Samanta, S., Pal, D.K., Palsamanta, B., 2018. Flood susceptibility analysis through remote sensing, GIS and frequency ratio model. Appl. Water Sci. 8, 66. doi:10.1007/s13201-018-0710-1

Sangireddy, H., Carothers, R.A., Stark, C.P., Passalacqua, P., 2016. Controls of climate, topography, vegetation, and lithology on drainage density extracted from high resolution topography data. J. Hydrol. 537, 271–282. doi:10.1016/j.jhydrol.2016.02.051

Santos, P.P., Pereira, S., Zêzere, J.L., Reis, E., Garcia, R.A.C., 2018. Flood susceptibility assessment based on Analytical Hierarchy Process: application in mainland Portugal. Geophys. Res. Abstr. 20, 85827.

Schumann, G.J.-P., Vernieuwe, H., De Baets, B., Verhoest, N.E.C., 2014. ROC-based calibration of flood inundation models. Hydrol. Process. 28, 5495–5502. doi:10.1002/hyp.10019

Shahabi, H., Shirzadi, A., Ghaderi, K., Omidvar, E., 2020. Flood Detection and Susceptibility Mapping Using Sentinel-1 Remote Sensing Data and a Machine Learning Approach : Hybrid Intelligence of Bagging Ensemble Based on K-

Nearest Neighbor Classifier. doi:10.3390/rs12020266

Singh, R.L., 1971. India: A Regional Geography, Silver jubilee publication. National Geographical Society of India.

Spyropoulos, N. V., Dalezios, N.R., Kaltsis, I., Faraslis, I.N., 2020. Very high resolution satellite-based monitoring of crop (olive trees) evapotranspiration in precision agriculture. Int. J. Sustain. Agric. Manag. Informatics 6, 22. doi:10.1504/IJSAMI.2020.106539

Sterckx, S., Brown, I., Kääb, A., Krol, M., Morrow, R., Veefkind, P., Boersma, K.F., De Mazière, M., Fox, N., Thorne, P., 2020. Towards a European Cal/Val service for earth observation. Int. J. Remote Sens. 41, 4496–4511. doi:10.1080/01431161.2020.1718240

Storn, R., 1999. System design by constraint adaptation and differential evolution. IEEE Trans. Evol. Comput. 3, 22–34. doi:10.1109/4235.752918

Storn, R., Price, K., 1995. Differential evolution–a simple and efficient adaptive scheme for global optimization over continuous spaces: technical report TR-95-012. Int. Comput. Sci. Berkeley, Calif.

Süzen, M.L., Doyuran, V., 2004. A comparison of the GIS based landslide susceptibility assessment methods: Multivariate versus bivariate. Environ. Geol. 45, 665–679. doi:10.1007/s00254-003-0917-8

Takagi, T., Sugeno, M., 1985. Fuzzy identification of systems and its applications to modeling and control. IEEE Trans. Syst. Man. Cybern. SMC-15, 116–132. doi:10.1109/TSMC.1985.6313399

1371 Tang, Q., Durand, M., Lettenmaier, D.P., Hong, Y., 2010. Satellite-based
1372 observations of hydrological processes. Int. J. Remote Sens. 31, 3661–3667.
1373 doi:10.1080/01431161.2010.483496

1374 Tebbens, L.A., Veldkamp, A., Westerhoff, W., Kroonenberg, S.B., 1999. Fluvial
1375 incision and channel downcutting as a response to Late-glacial and Early
1376 Holocene climate change: the lower reach of the River Meuse (Maas), The
1377 Netherlands. J. Quat. Sci. 14, 59–75. doi:10.1002/(SICI)1099-
1378 1417(199902)14:1<59::AID-JQS408>3.0.CO;2-Z

1379 Tehrany, M.S., Jones, S., Shabani, F., 2019. Identifying the essential flood
1380 conditioning factors for flood prone area mapping using machine learning
1381 techniques. Catena 175, 174–192. doi:S0341816218305472

1382 Tehrany, M.S., Pradhan, B., Jebur, M.N., 2013. Spatial prediction of flood
1383 susceptible areas using rule based decision tree (DT) and a novel ensemble
1384 bivariate and multivariate statistical models in GIS. J. Hydrol. 504, 69–79.
1385 doi:10.1016/j.jhydrol.2013.09.034

1386 Tehrany, M.S., Pradhan, B., Mansor, S., Ahmad, N., 2015. Flood susceptibility
1387 assessment using GIS-based support vector machine model with different
1388 kernel types. Catena. doi:10.1016/j.catena.2014.10.017

1389 Testa, F., Gusmerottia, N.M., Corsini, F., Passetti, E., Iraldo, F., 2016. Factors
1390 Affecting Environmental Management by Small and Micro Firms: The
1391 Importance of Entrepreneurs' Attitudes and Environmental Investment. Corp.
1392 Soc. Responsib. Environ. Manag. 23, 373–385. doi:10.1002/csr.1382

1393 Thies, B., Bendix, J., 2011. Satellite based remote sensing of weather and climate:

recent achievements and future perspectives. Meteorol. Appl. 18, 262–295. doi:10.1002/met.288

Tien Bui, D., Nguyen, Q.P., Hoang, N.D., Klempe, H., 2017. A novel fuzzy K-nearest neighbor inference model with differential evolution for spatial prediction of rainfall-induced shallow landslides in a tropical hilly area using GIS. Landslides 14. doi:10.1007/s10346-016-0708-4

Tien Bui, D., Pradhan, B., Nampak, H., Bui, Q.T., Tran, Q.A., Nguyen, Q.P., 2016. Hybrid artificial intelligence approach based on neural fuzzy inference model and metaheuristic optimization for flood susceptibilitgy modeling in a high-frequency tropical cyclone area using GIS. J. Hydrol. doi:10.1016/j.jhydrol.2016.06.027

Tonetti, S., Cornara, S., Vicario de Miguel, G., Pierotti, S., Cote, J., Araguz, C., Alarcón, E., Camps, A., Llaveria, D., Lancheros, E., Ruiz-de-Azua, J.A., Bou-Balust, E., Rodríguez, P., Sochacki, M., Narkiewicz, J., Golkar, A., Lluch i Cruz, I., Matevosyan, H., 2020. Mission and system architecture for an operational network of earth observation satellite nodes. Acta Astronaut. 176, 398–412. doi:10.1016/j.actaastro.2020.06.039

Übeyli, E.D., Cvetkovic, D., Holland, G., Cosic, I., 2010. Adaptive neuro-fuzzy inference system employing wavelet coefficients for detection of alterations in sleep EEG activity during hypopnoea episodes. Digit. Signal Process. 20, 678–691. doi:https://doi.org/10.1016/j.dsp.2009.08.005

UNSDG, 2013. Open Working Group proposal for Sustainable Development Goals [WWW Document]. United Nations Sustain. Dev. Goals. URL

https://sustainabledevelopment.un.org/focussdgs.html

Vittal, H., Ghosh, S., Karmakar, S., Pathak, A., Murtugudde, R., 2016. Lack of Dependence of Indian Summer Monsoon Rainfall Extremes on Temperature: An Observational Evidence. Sci. Rep. 6, 1–12. doi:10.1038/srep31039

Wang, J., Bhattacharya, J.P., 2017. Plan-view Paleochannel Reconstruction of Amalgamated Meander Belts, Cretaceous Ferron Sandstone, Notom Delta, South-central Utah, U.s.a. J. Sediment. Res. 88, 58–74. doi:10.2110/jsr.2017.77

Wang, Y., Fang, Z., Hong, H., Peng, L., 2020. Flood susceptibility mapping using convolutional neural network frameworks. J. Hydrol. 582, 124482. doi:10.1016/j.jhydrol.2019.124482

Wei, M., Bai, B., Sung, A.H., Liu, Q., Wang, J., Cather, M.E., 2007. Predicting injection profiles using ANFIS. Inf. Sci. (Ny). 177, 4445–4461. doi:10.1016/j.ins.2007.03.021

Williams, G.P., 1978. Bank-full discharge of rivers. Water Resour. Res. 14, 1141–1154. doi:10.1029/WR014i006p01141

Yevjevich, V., 1994. Floods and society, in: Coping with Floods. Springer Netherlands, Dordrecht, pp. 3–9. doi:10.1007/978-94-011-1098-3_1

Zabihi, M., Pourghasemi, H.R., Motevalli, A., Zakeri, M.A., 2019. Gully erosion modeling using gis-based data mining techniques in Northern Iran: a comparison between boosted regression tree and multivariate adaptive regression spline. Adv. Nat. Technol. Hazards Res. 48, 1–26. doi:10.1007/978-3-319-73383-8_1

Zhang, K., Gann, D., Ross, M., Robertson, Q., Sarmiento, J., Santana, S., Rhome, J., Fritz, C., 2019. Accuracy assessment of ASTER, SRTM, ALOS, and TDX DEMs for Hispaniola and implications for mapping vulnerability to coastal flooding. Remote Sens. Environ. 225, 290–306. doi:10.1016/j.rse.2019.02.028

List of figures

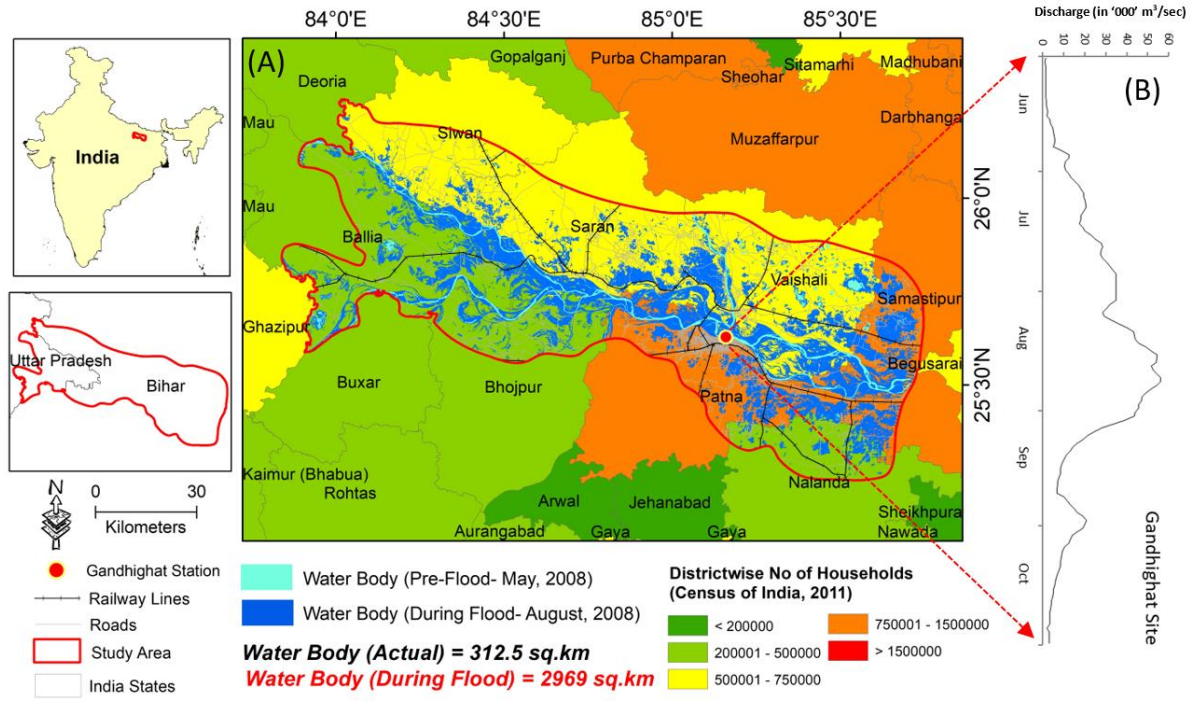

Figure 1: (A) Location map of Middle Ganga Plain (MGP); (B) Mean monthly discharge during monsoon period (Jun to October) at Gandhighat station for 2008 year.

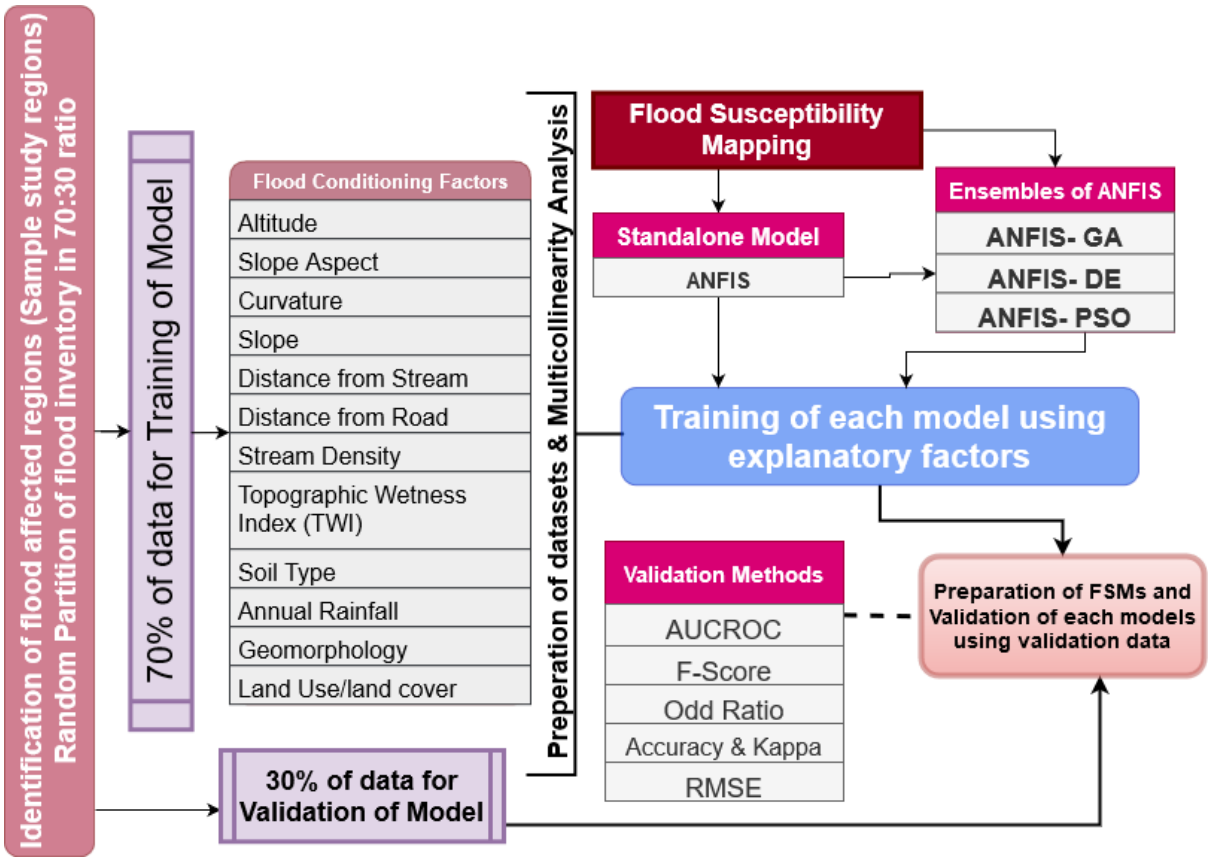

Figure 2: Flowchart of methodological steps followed in this work

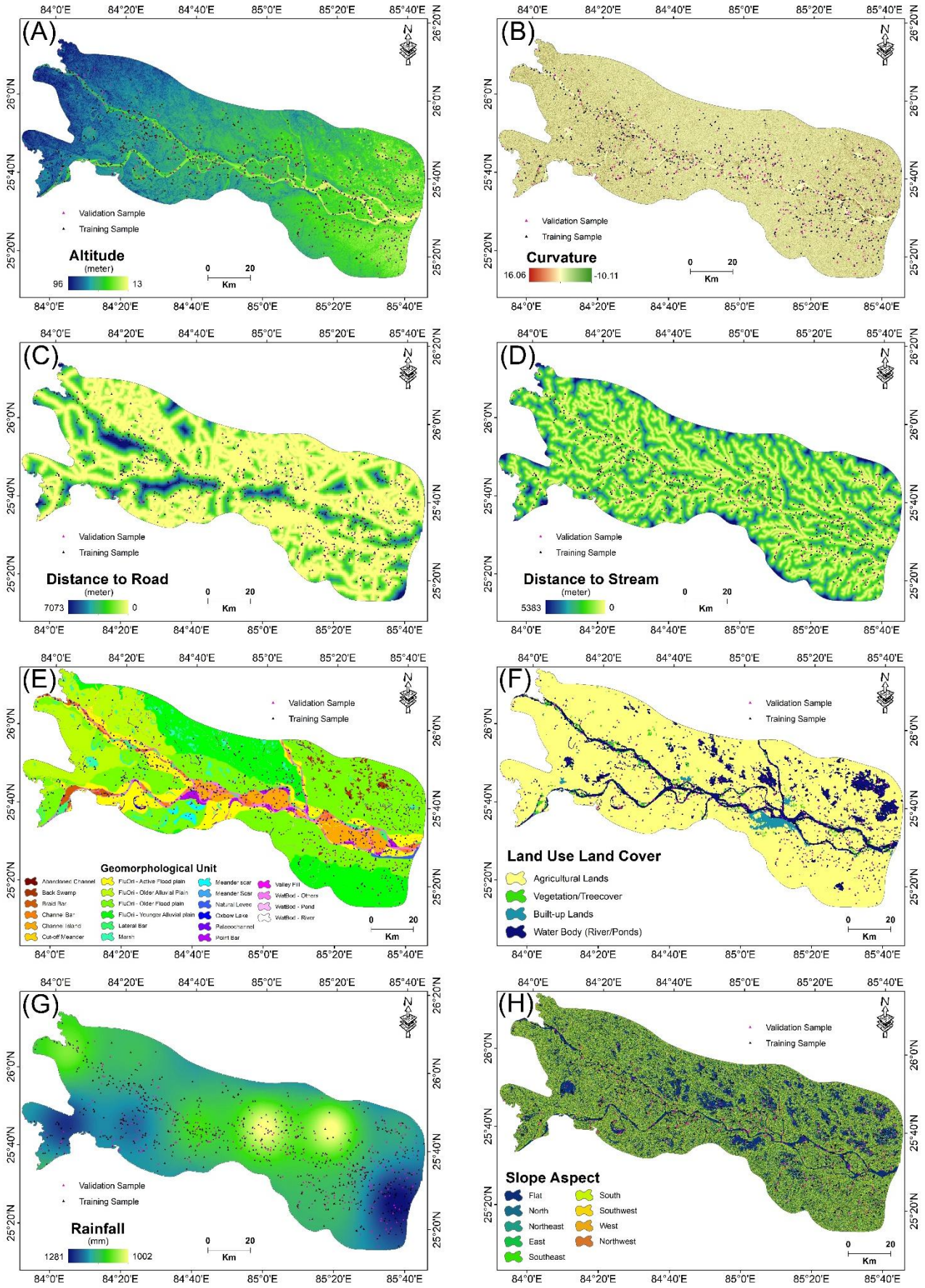
(A)
Validation Sample
Training Sample
Altitude
(meter)
96
13
(B)
Curvature
16.06
-10.11
(C)
Distance to Road
7073
0
(D)
Distance to Stream
5383
0
(E)
Geomorphological Unit
Abandoned Channel
Back Swamp
Braid Bar
Channel Bar
Channel Island
Cut-off Meander
FluDel - Active Flood plain
FluDel - Older Alluvial Plain
FluDel - Older Flood plain
FluDel - Younger Alluvial plain
Lateral Bar
Marsh
Meander scar
Meander Scar
Natural Levee
Oxbow Lake
Paleochannel
Point Bar
Valley Fill
WatBod - Others
WatBod - Pond
WatBod - River
(F)
Land Use Land Cover
Agricultural Lands
Vegetation/Treecover
Built-up Lands
Water Body (River/Ponds)
(G)
Rainfall
(mm)
1281
1002
(H)
Slope Aspect
Flat
North
Northeast
East
Southeast
South
Southwest
West
Northwest
0
20
Km
84°0'E
84°20'E
84°40'E
85°0'E
85°20'E
85°40'E
26°0'N
25°40'N
25°20'N

1456

Figure 3: Continues

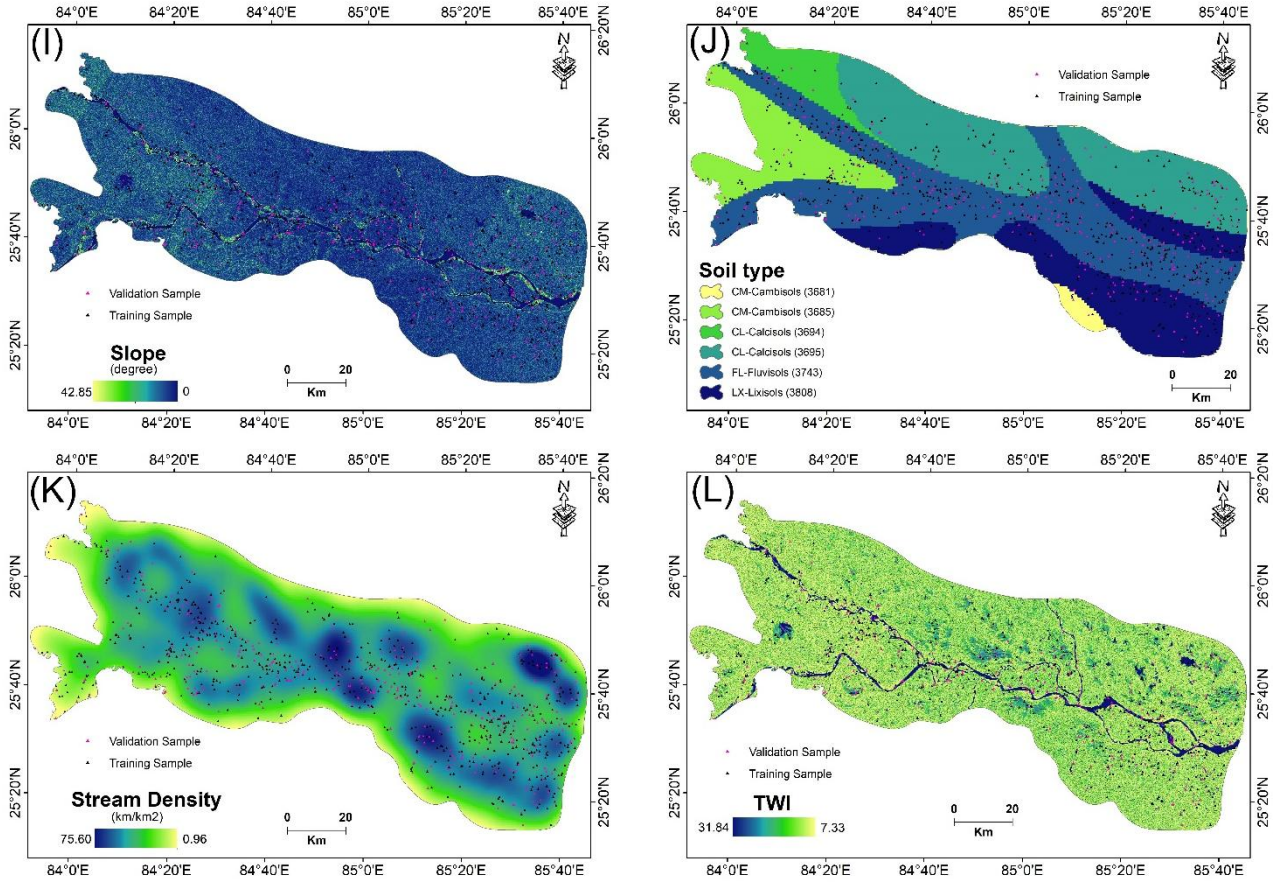

Figure 3: Flood conditioning factors. From A to L the maps indicate: Altitude; Curvature; Distance to Road; Distance to Stream; Geomorphology; Land Use Land Cover; Rainfall; Slope Aspect; Slope; Soil Type; Stream Density; and Topographical Wetness Index (TWI).

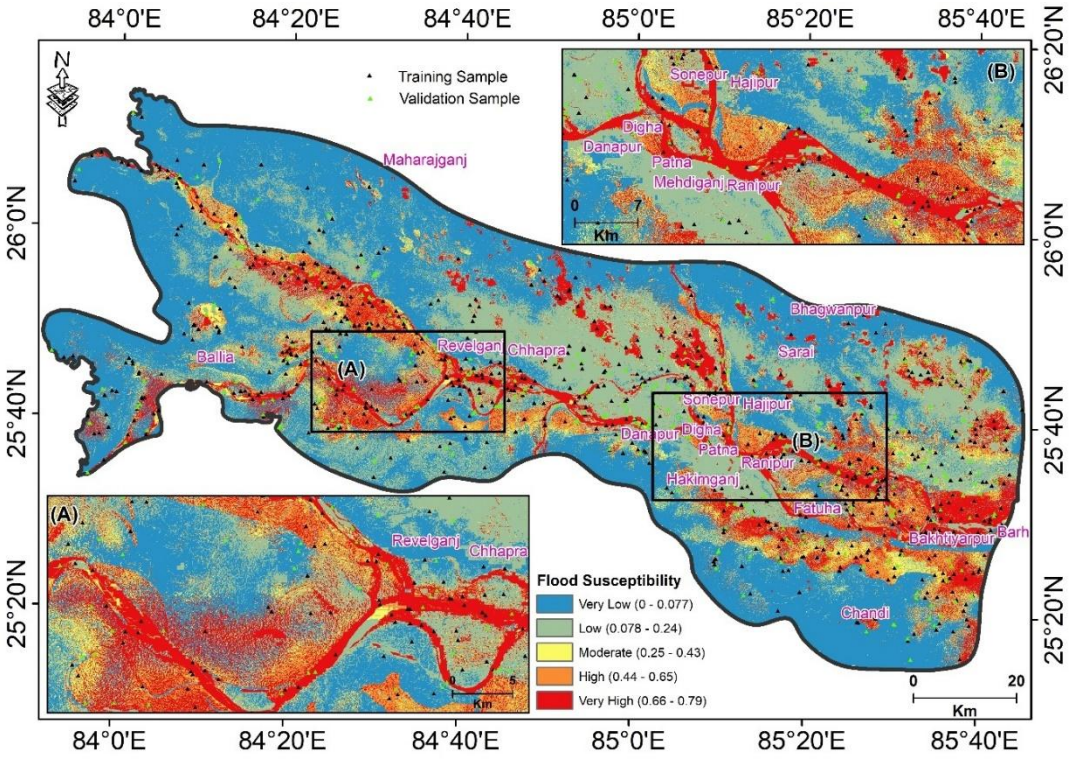

1464

1465 **Figure 4:** Flood susceptibility mapping using ensemble of adaptive neuro-fuzzy
1466 inference system (ANFIS) model

1467

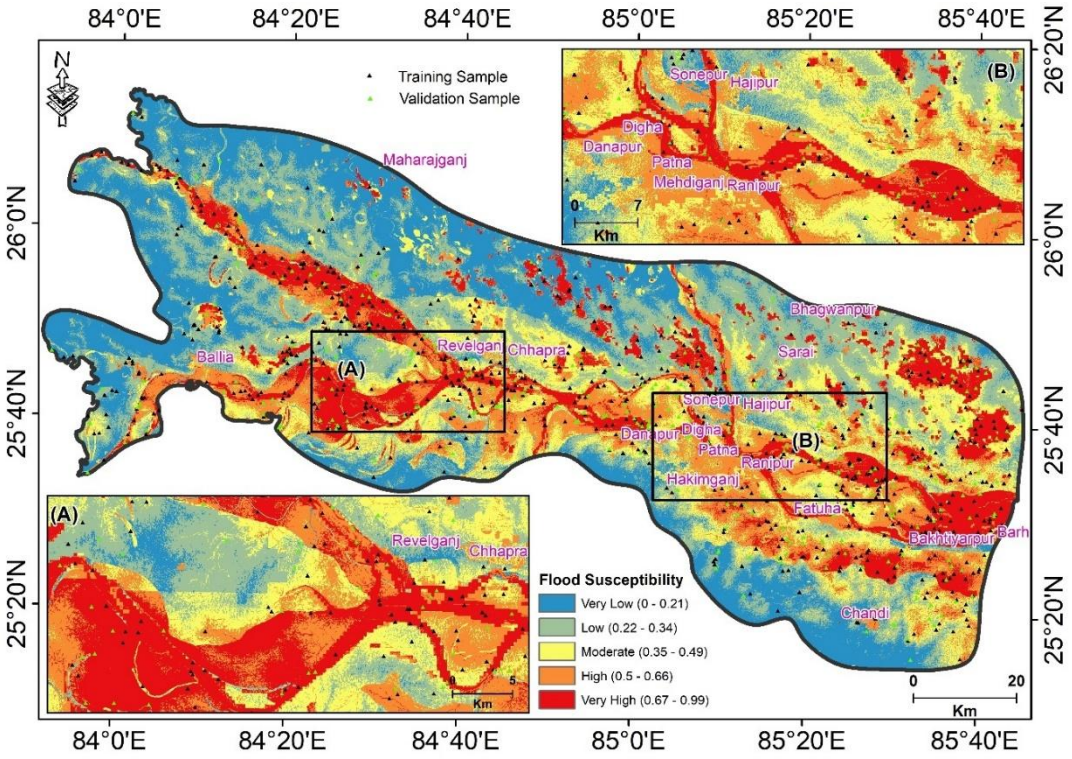

1468

1469 **Figure 5:** Flood susceptibility mapping using ensemble of adaptive neuro-fuzzy
1470 inference system (ANFIS) model with genetic algorithm (GA)

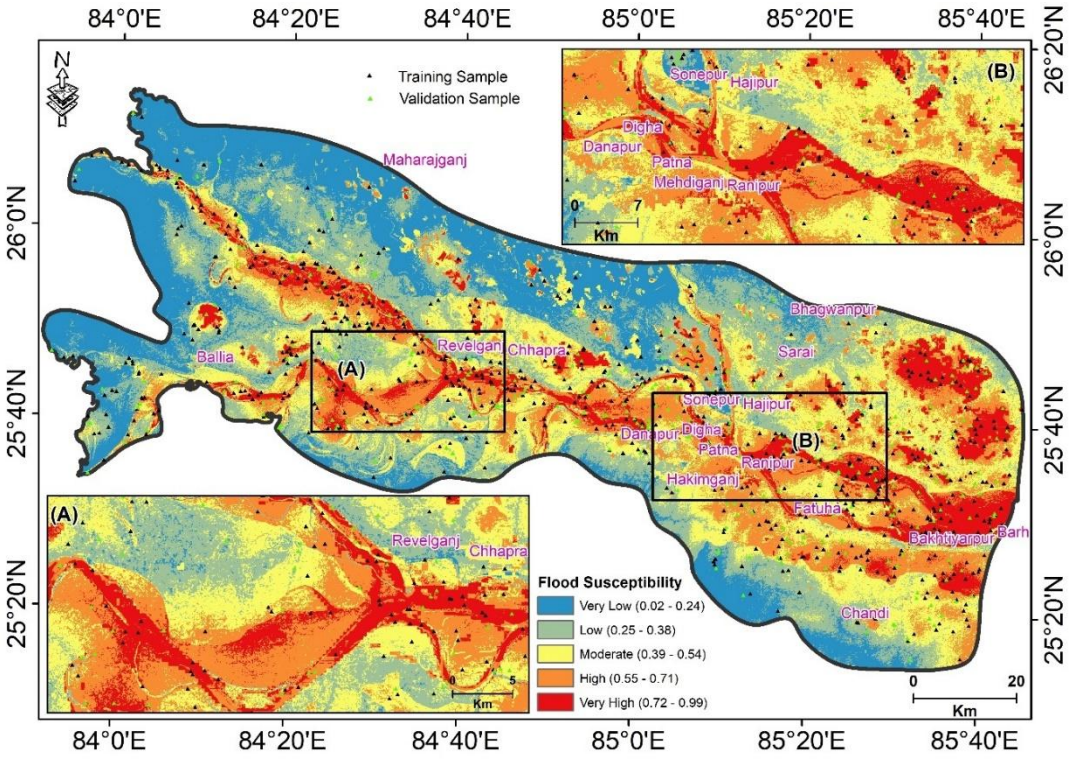

Figure 6: Flood susceptibility mapping using ensemble of adaptive neuro-fuzzy inference system (ANFIS) model with a) differential evolutionary (DE)

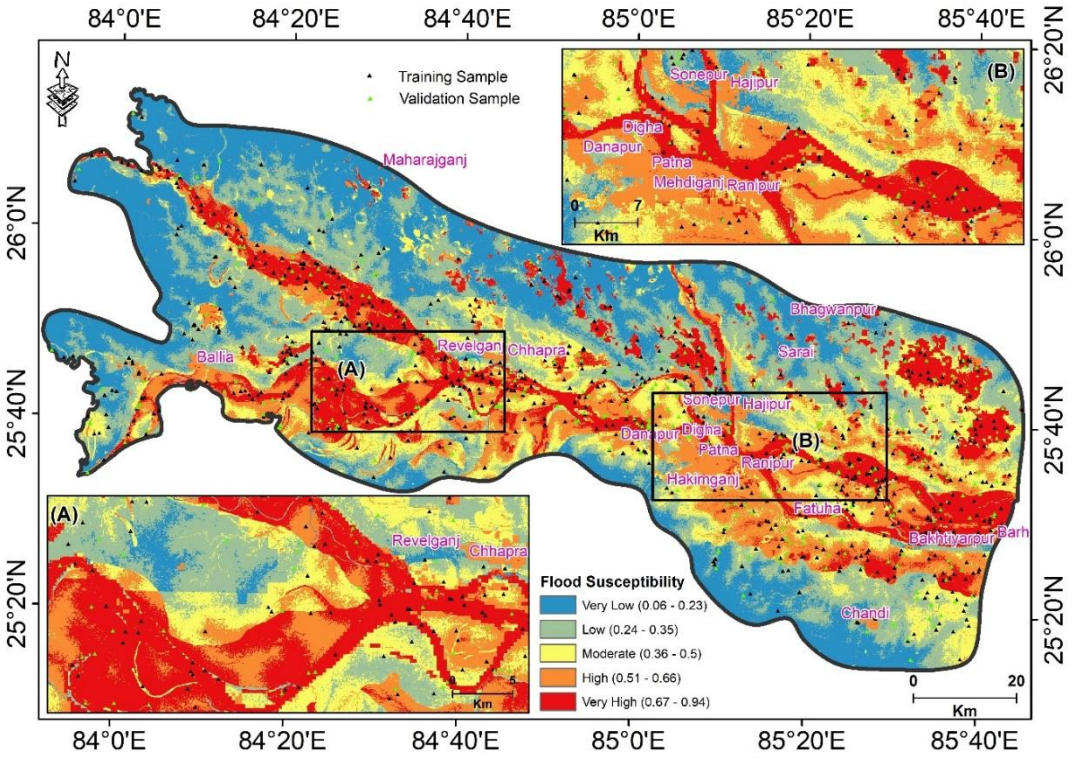

Figure 7: Flood susceptibility mapping using ensemble of adaptive neuro-fuzzy inference system (ANFIS) model with particle swarm optimization (PSO)

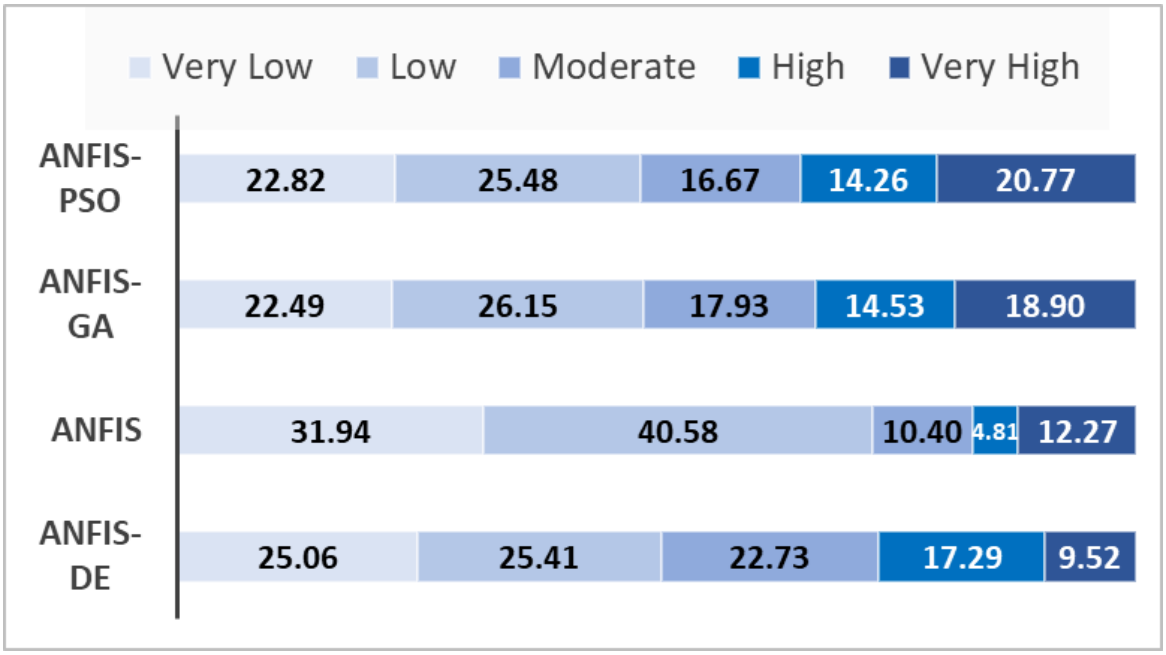

Figure 8: Percentage of each susceptibility classes classified using natural break in all models' results

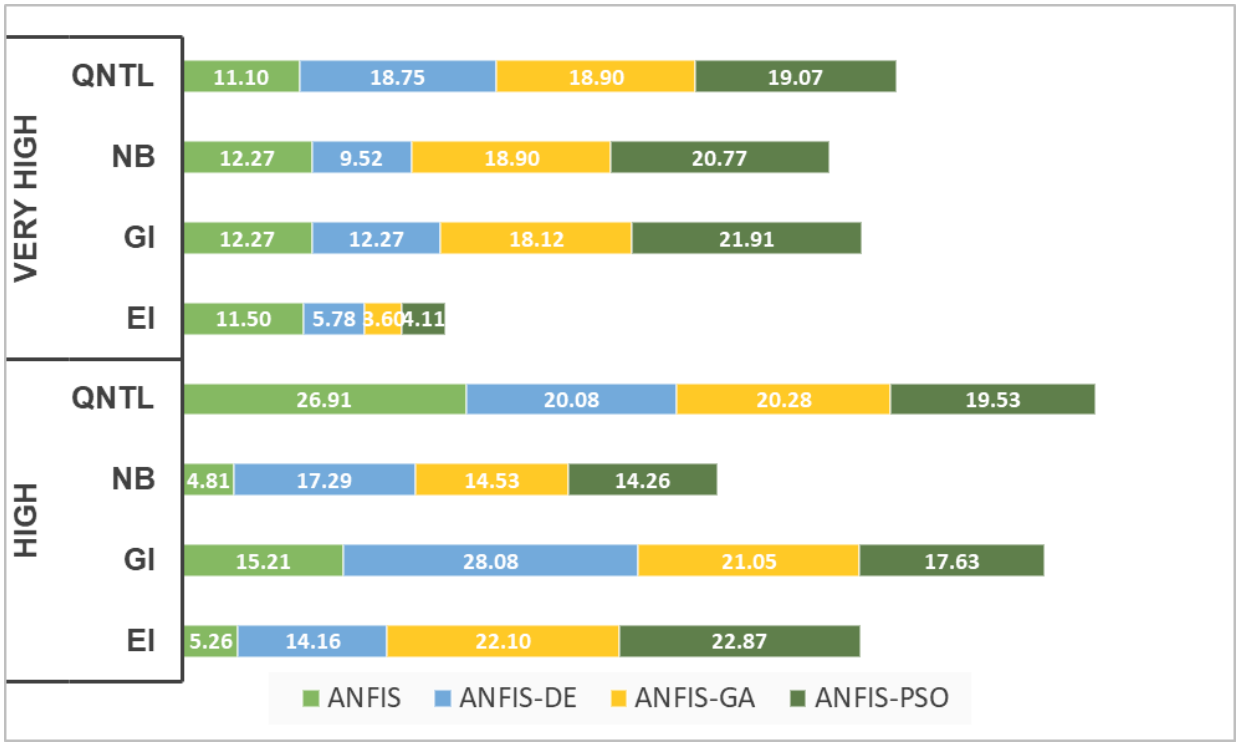

Figure 9: Percentage of 'High' & 'Very High' susceptibility classes of flood susceptibility potential mapping as per all the models suing different classification methods (QNTL=Quantile; NB=Natural Break; GI=Geometric Interval; EI= Equal Interval)

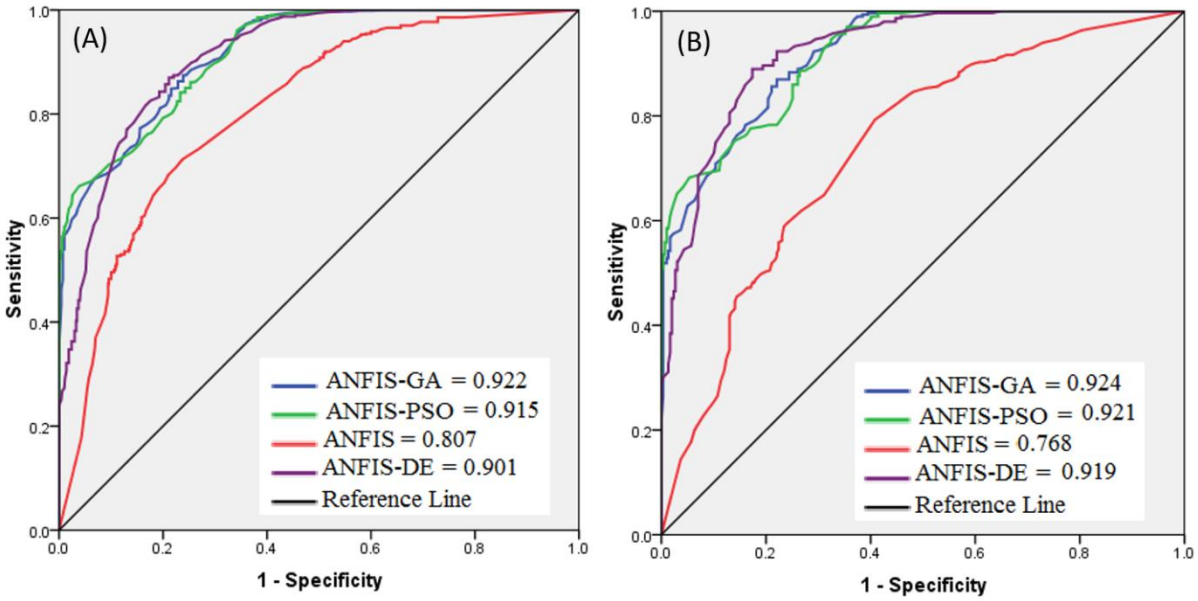

Figure 10: Area under the receiver operating characteristic (ROC) curves for all the models; Section (A) is with training data (success rate curve) and section (B) has been constructed with the validation data (prediction rate curve).

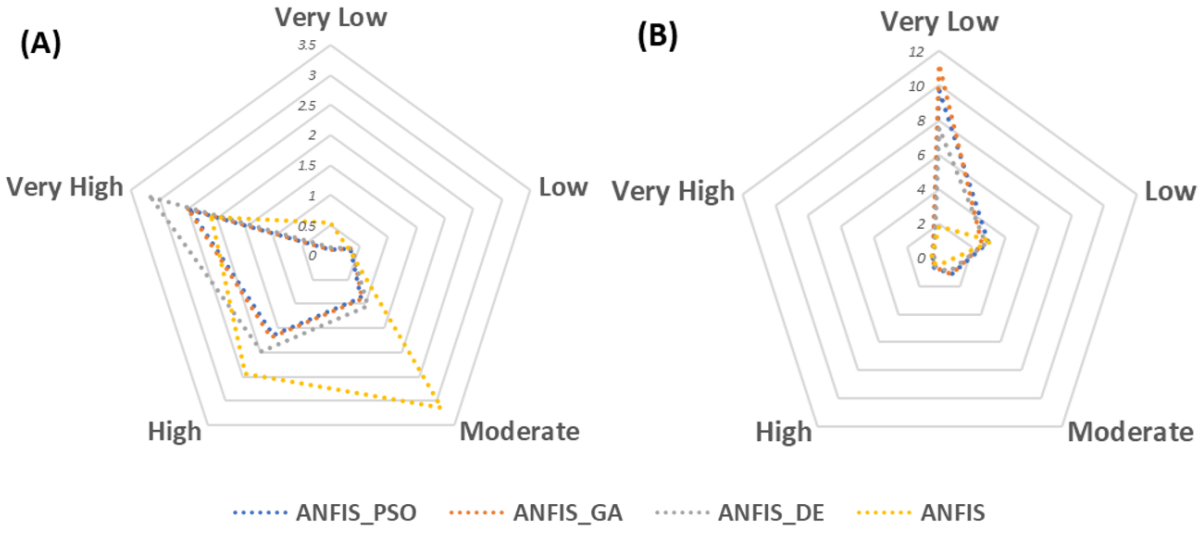

Figure 11: Validation of results using (A) frequency ratio (FR) and (B) seed cell area index (SCAI)

List of tables

Table 1: Details of satellite data used in the study

SN	Event time	Satellite (Spatial Resolution)	Acquisition date	Spatial reference (Projected)
1	Preflood	Landsat 5 TM (30-meter)	28-05-2008	Projection: UTM
2	During Flood		01-09-2008	
3	Post Flood		19-10-2008	Datum: WGS84
4	----	SRTM v4 DEM (1-arc or 30-meter)	11-22 Feb 2000	Spheroid: WGS84 Zone: 44N

Table 2: Geomorphological units in study area mapped and used in the modelling as one of the input conditioning factors

S. No.	Geomorphic Unit	Description
1.	FluOri - Active Flood plain	Junk *et al.*(1989) have presented, following Bhowmik & Stall (1979), active floodplain in technical terms and stated that the areas flooded by 100-year flood can be demarcated to be under the active floodplain zone. Active floodplain an overflown surface, usually, on either side of a streamwhich is periodically flooded and experiences both erosional and depositional processes building and destroying the surfaces but net result is net surface growth through the accretion of the depositional material (Williams, 1978). It should be noted that some river reaches do not have these active floodplain surfaces. These geomorphological units have high flood susceptibility as compared to older floodplain surfaces also termed as terraces.
2.	Meander scar	Meander scar is a crescent-shaped fossilized meandering channel segment currently covered with vegetation but with conspicuously visible channel geometry in the satellite imagery. Such geomorphic features represent low lying areas exposed to more susceptibility to

		flooding (Harris, 1987).
3.	Braid Bar	Any type of fluvial channel bars are in-channel depositonal features that show proportional length to the channel width and their hieghts can be comparable to channel depth of channel at bankfull stage (Lunt and Bridge, 2004). These geomorphic units, being in-active-channel features are comparably more flood susceptibility exposed members.
4.	Lateral Bar/lateral channel bar	The channel bar formed by the lateral aggradation process of fluvial deposition and reveals fining up trend of grain size depositional setting (Hudson, 2017). Being located along the active channel banks makes these fluvigenic geomorphic units one of the higher flood susceptible areas.
5.	Marsh	Riverine lowlying wetlands usually covered with vegetation classes with dominance of reeds and grasses.
6.	Channel Island	Mid channel large bars covered with vegetation providing stability to this geomorphic unit. Their sizes reach upto 100s km long and 10s km wide (Alabyan and Chalov, 1998).
7.	Paleochannel	Remnant of an inactive or non-functional river channel,characterized by younger sediment deposits burying the original geometry of the ancient channel is termed paleochannel (Wang and Bhattacharya, 2017).
8.	WatBod - Pond	Large and small depression in the river valley filled with water through natural/ or later revived through artificial recharge process are called ponds. The ponds are smaller than lakes. Geomorphologically, those large/small depressions present in the river valley are ponds.
9.	FluOri - Older Flood plain	Surfaces within the river valleys exposed to different hydrological regime or uplifted due to active tectonic regime become discordant to annual flooding or regular flooding and can be called as older alluvial floodplain. Or in other words, the disconnected floodplain surfaces from main river channels, which mostly lie on higher altitude than present active annually or regularly inundated floodplains are termed olderfloodplains. Due to distant proximity to main channels the chances of inundation of older floodplains are very low and these geomorphic units are preferred for habitation and infrastructure establishment.
10.	Abandoned Channel	River channels no longer part of the current flowing channel either because of channel avulsion, or meander neck cutting, or any other reason, are termed abandoned channels. These are important geomorphic units in the fluvial landscape ecosystem and are prone to flooding (Field, 2001).

11.	Point Bar	A type of river channel bar found along the convex banks of river bends. These are annually flooded during the high flow regime.
12.	FluOri - Older Alluvial Plain	The older alluvium depositions are referred as older alluvial plain.
13.	Channel Bar	Channel bar is the common term in the fluvial lexicon and refers to any type of bar deposits by the river flow. The channel bars are formed due to high sediments yield in the channels and they are characterized by coarse sand, pebbles and boulders.
14.	WatBod - River	The main and active flowing watercourses are called rivers. Stream is the technical term which refers to concentrated linear flow of water in channelized form.
15.	Cut-off Meander	These landforms are formed when the meander neck is narrowed to a certain extent and finally cuts to shorten the course of the stream; generally this takes place due to lateral bank erosion process.
16.	Backswamp	Low lying depressional areas located in the floodplains adjacent to the river channel levees and sedimentologically, characterized by fine silts and clays sized particles. These geomorphic features areformed after occurrence overtopping or transcendental flow of flood waters through arroyos and debouching their fine silt- and clay-sized deposits in a floodplain; generally behind natural levees. The geomorphic processes signify their susceptibility to either annual flooding or extreme flooding.
17.	Valley Fill	In fluvial depositional environments, the valley fills are depositional units formed after a partial or complete fill of a valley by unconsolidated suspended and dissolved load carried by the river flow.
18.	Oxbow Lake	When the meandering flow path of the river is abandoned by meander neck cutting process, the cut-off segment of the channel with meander planform geometry, normally supported with groundwater as well as rain water and floodwater for the water inflow, this landform unit with U-shaped lake forms.
19.	Natural Levee	A generally discontinuous natural embankment almost parallel to the channel flow direction is formed by sediment deposited by the natural flow of water on eitherside of channel. This unit has lower flood susceptibility as compared to the in-channel bars.
20.	FluOri - Younger Alluvial plain	River channel incision caused by different set of factors forces the incised river to inundate lesser areas. Some part of the repeatedly flooded zones which were previously under flood during rainy season remains dry. And this wet-dry transition zone between periodically flooded and non-flooded zones defines the younger and older floodplains (Jacobson and Faust, 2014; Tebbens et al., 1999). The

		repeatedly flooded zone, on both sides channel banks, adjacent to the current active channel which get annual alluvial deposits marks the younger alluvial floodplain.
21.	WatBod - Others	Other smaller waterbodies other than river and pond.

1503

1504 Note: The data source is the Geological Survey of India, Government of India official portal
1505 (http://bhukosh.gsi.gov.in/), but the contents of this map has been prepared and updated by
1506 author using different sources

1507

Table 3: Multicollinearity Analysis of the flood conditioning factors

S. No.	Conditioning Factors	Collinearity Statistics	
		Tolerance	VIF
1.	Altitude (Al)	0.538	1.858
2.	Curvature (Cr)	0.924	1.082
3.	Distance to Roads (D2R)	0.926	1.079
4.	Distance to Streams (D2S)	0.776	1.289
5.	Geomorphology (G)	0.913	1.095
6.	Land Use Land Cover (LULC)	0.707	1.415
7.	Rainfall (Rf)	0.906	1.103
8.	Slope (Sl)	0.749	1.336
9.	Slope Aspect (SA)	0.874	1.145
10.	Soil (S)	0.784	1.276
11.	Stream Density (SD)	0.733	1.365
12.	Topographic Wetness Index (TWI)	0.623	1.605

Table 4: Confusion matrix from the RF model (1 = flood, 0 = non-flood)

	0	**1**
0	325	167
1	130	357

Table 5: Relative influence of effective conditioning factors in the RF model

S. No.	Factor	Relative weight	Rank
1.	Altitude (Al)	0.07	10
2.	Curvature (Cr)	0.10	3
3.	Distance to Roads (D2R)	0.07	8

4.	Distance to Streams (D2S)	0.12	2
5.	Geomorphology (G)	0.13	1
6.	Land Use Land Cover (LULC)	0.08	6
7.	Rainfall (Rf)	0.04	12
8.	Slope (Sl)	0.10	4
9.	Slope Aspect (SA)	0.07	9
10.	Soil (S)	0.05	11
11.	Stream Density (SD)	0.09	5
12.	Topographic Wetness Index (TWI)	0.07	7

Table 6: Validation of results by model evaluation metrices

Data	Criteria	ANFIS-PSO	ANFIS	ANFIS-DE	ANFIS-GA
Training data	True Negative (TN)	613	593	608	621
	False Positive (FP)	87	107	92	79
	False Negative (FN)	93	96	93	80
	True Positive (FP)	607	604	607	620
	Accuracy	0.871	0.855	0.868	0.886
	Precision	0.876	0.847	0.869	0.887
	Sensitivity	0.867	0.863	0.867	0.886
	Specificity	0.876	0.847	0.869	0.887
	False Positive Rate	0.1243	0.1505	0.1316	0.1130
	False Discovery Rate	0.1254	0.1529	0.1314	0.1129
	False Negative Rate	0.1329	0.1393	0.1327	0.1141
	F-Score	0.871	0.856	0.868	0.886
	Odd ratio	45.988	34.869	43.134	60.921
	Cohens kappa	0.743	0.710	0.736	0.773
	AUCROC	0.915	0.807	0.901	0.922
	RMSE	0.402	0.413	0.410	0.398
Validation data	True Negative (TN)	265	258	260	270
	False Positive (FP)	35	42	40	30
	False Negative (FN)	40	46	43	40
	True Positive (FP)	260	254	257	260
	Accuracy	0.875	0.853	0.862	0.883
	Precision	0.883	0.860	0.867	0.900
	Sensitivity	0.867	0.847	0.857	0.867
	Specificity	0.883	0.860	0.867	0.900
	False Positive Rate	0.1186	0.1419	0.1347	0.1034
	False Discovery Rate	0.1167	0.1400	0.1333	0.1000
	False Negative Rate	0.1311	0.1513	0.1419	0.1290
	F-Score	0.874	0.852	0.861	0.881
	Odd ratio	49.214	33.919	38.849	58.500
	Cohens kappa	0.750	0.707	0.723	0.767
	AUCROC	0.921	0.768	0.919	0.924
	RMSE	0.379	0.390	0.387	0.375